NASA-CR-201390
NASA Grant NAG-1-1509

Evaluation of Subgrid-Scale Models for Large Eddy Simulation of Compressible Flows

Gregory A. Blaisdell
School of Aeronautics & Astronautics
Purdue University
1282 Grissom Hall
West Lafayette, IN 47907-1282

May 22, 1996

Final Technical Report for Period May 6, 1993 – November 5, 1995

Prepared for:
Dr. Thomas B. Gatski
NASA Langley Research Center
Mail Stop 128
Hampton, VA 23681-0001

Contents

1 Overview

This report summarizes a project sponsored by the NASA Langley Research Center through the Langley Grad-Aero Program under Grant No. NAG-1-1509. The project was approved for the period May 6, 1993 - November 4, 1997. However, due to reductions in NASA's budget and limited funds for the Grad-Aero Program, funding was halted in November 1994. A one-year no-cost extension was requested so that the student could attend the AIAA 1995 Aerospace Sciences Meeting. During that period supplemental funding was made available to support the student over the summer of 1995. The extended termination date for the NASA grant was November 5, 1995. The project has been continued by supporting the student as a Teaching Assistant within the School of Aeronautics and Astronautics. Although funding for this project was terminated, NASA Langley has continued to provide access to their computer facilities.

The objective of this project was to evaluate and develop subgrid-scale (SGS) turbulence models for large eddy simulations (LES) of compressible flows. During the first phase of the project results from LES using the dynamic SGS model were compared to those of direct numerical simulations (DNS) of compressible homogeneous turbulence. The findings were published in Ref. [1-3]. Ref. [3] is included in this report as Attachment A.

It is becoming apparent within the LES community that numerical errors can have a significant impact on large eddy simulations. Ref. [4] reports results of a study on the effect of the formulation of the governing equations on aliasing errors. A copy of the galley proof for this paper is included as Attachment B.

The second phase of the project involved implementing the dynamic SGS model in a NASA code for simulating supersonic flow over a flat-plate. The model has been successfully coded and a series of simulations has been completed. One of the major findings of the work is that numerical errors associated with the finite differencing scheme used in the code can overwhelm the SGS model and adversely affect the LES results. A brief write-up of the results [5] has been submitted to the AIAA 1997 Aerospace Sciences Meeting and is included as Attachment C.

One of the goals of the Langley Grad-Aero Program is to train young researchers in Aerospace Engineering and related fields. The student supported by this project, Evangelos T. Spyropoulos, has performed very well. He has grown as a researcher in the very difficult field of turbulence. In 1993 he participated in the ICASE/NASA Langley summer workshop on Transition, Turbulence and Combustion. He again visited NASA Langley during the summers of 1994 and 1995. It has been very beneficial for him to interact with NASA personnel and with NASA visitors from all over the world. Evangelos is currently finishing his Ph.D. dissertation and should graduate this August. He is looking forward to a career in the aerospace industry where he can put his understanding to good use.

2 References

[1] Spyropoulos, E. T. and Blaisdell, G. A., Evaluation of Inhomogeneous Formulations of the Dynamic Subgrid-Scale Model. In *Transition, Turbulence and Combustion*, Vol. II (eds. M. Y. Hussaini, T. B. Gatski, and T. L. Jackson), Kluwer Academic Publishers, (1993) pp. 51–60.

[2] Spyropoulos, E. T. and Blaisdell, G. A., Evaluation of the Dynamic Subgrid-Scale Model for Large Eddy Simulation of Compressible Turbulent Flows. AIAA Paper 95-0355. Presented at the 33rd AIAA Aerospace Sciences Meeting, Reno, NV, January 1995.

[3] Spyropoulos, E. T. and Blaisdell, G. A., Evaluation of the Dynamic Model for Simulations of Compressible Decaying Isotropic Turbulence, *AIAA Journal*, Vol. 34, May 1996, pp. 990–998.

[4] Blaisdell, G. A., Spyropoulos, E. T., and Qin J. H., The Effect of the Formulation of Nonlinear Terms on Aliasing Errors in Spectral Methods. To appear in *Applied Numerical Mathematics*, November 1996.

[5] Spyropoulos, E. T. and Blaisdell, G. A., Large-Eddy Simulation of a Spatially Evolving Compressible Boundary Layer Flow. Extended abstract submitted to the AIAA 1997 Aerospace Sciences Meeting.

Attachment A

AIAA JOURNAL
Vol. 34, No. 5, May 1996

Evaluation of the Dynamic Model for Simulations of Compressible Decaying Isotropic Turbulence

Evangelos T. Spyropoulos* and Gregory A. Blaisdell†
Purdue University, West Lafayette, Indiana 47907

Several issues involving the use of the dynamic subgrid-scale model in large-eddy simulations of compressible turbulent flows are investigated. The model is employed in simulations of compressible decaying isotropic turbulence, and its performance is compared against results from direct numerical simulations and experiments. Results from a parametric study suggest the model captures compressibility effects well. Use of the dynamic model in simulations of inhomogeneous flows requires filtering of the flowfield in physical space rather than Fourier wave space. The use of spatial filters is examined by conducting simulations of isotropic turbulence. Several implicit filters are found to perform extremely well and similar to the sharp cutoff filter. One explicit filter performed well, but all others provided excessive dissipation at higher modes. Two formulations of the dynamic model, proposed by Moin et al. and Lilly, perform well, with Lilly's being more accurate. Results suggest also a great insensitivity of the model on the filter width ratio. A modification of the convective terms in the momentum and energy equations is found to reduce the effects of aliasing errors. Finally, different formulations of the energy equation are examined. A nonconservative form is found to be more accurate.

I. Introduction

In the past few years there has been a resurgence of interest in performing large-eddy simulations (LES) of flows of engineering interest. There are two roles for LES to play in the computation of such flows. First, LES can be used to test lower order models: k–ϵ, algebraic stress, and full Reynolds stress models. LES can provide detailed data, which is difficult or impossible to measure experimentally and which is at much higher Reynolds numbers than can be reached by direct numerical simulation (DNS). Statistical data and physical insight gained from these simulations can be used to evaluate and improve the lower order models. With this approach, however, the subgrid-scale (SGS) model used in the LES has to be validated in order to ensure that the LES data are correct.

Second, LES can be used as an engineering tool rather than as a research tool. With the expected increases in computer capabilities in the near future, especially from the use of massively parallel computers, it may be feasible to perform LES of flows of engineering interest. LES will remain an expensive tool, but it will likely be the only means of accurately computing complex flows for which lower order turbulence models fail.

Recently, there has been much interest in using the dynamic SGS model to perform LES. The dynamic model was first introduced by Germano et al.[1] and was extented for use in compressible flows by Moin et al.[2] Since then, further refinements to the model have been proposed.[3–6] The main advantage of the dynamic model over other SGS models used in the past is that it requires little prior experience with the type of flow being considered. The model (dynamically) adjusts to the flow conditions by employing the resolved large-scale information to predict the effects of the small scales.

So far, the dynamic model has been mostly tested in incompressible turbulent flows and has been found to perform well. Moin et al.[2] applied the dynamic model to compressible decaying isotropic turbulence and found that it performed well and better than using fixed values for the model constants. El Hady et al.[7] applied the model to a transitional supersonic axisymmetric boundary layer with satisfactory results. However, a number of issues regarding the use of the model in LES of compressible turbulence remain to be addressed, such as the ability of the model to capture compressibility effects without the need for explicit compressibility corrections.

In addition, there are issues that need to be addressed in applying the dynamic model to inhomogeneous flows. The dynamic model requires filtering the resolved large-scale field. So far, it has been mostly implemented in turbulent flows that are homogeneous in at least two directions where the filtering can be performed efficiently (and exactly) in wave space using fast Fourier transforms. In more complex inhomogeneous flows, this is not possible, and some kind of discrete filtering has to be applied in physical space. In simulations of such flows, three-point explicit filters have been mostly used. A number of other spatial filters are available and require testing.

The main objective of this paper is to examine the performance of the dynamic SGS model in the context of compressible decaying isotropic turbulence. The model is evaluated by making comparisons with results from direct numerical simulations, as well as with reported "high" Reynolds number, nearly incompressible experimental data. The simulations are used to assess the capture of compressibility effects and to investigate issues regarding the implementation of the dynamic model for inhomogeneous flows. The reason for considering homogeneous turbulence is that the performance of the dynamic model can be evaluated separately from the effects of inhomogeneity.

II. Mathematical Formulation

A. Governing Equations

In LES one computes the motion of the large-scale structures, while modeling the nonlinear interactions with the small scales. The governing equations for the large eddies in compressible flows are obtained after filtering the continuity, momentum, and energy equations and recasting in terms of Favre averages. The filtering operation (denoted by an overbar) maintains only the large scales and can be written in terms of a convolution integral,

$$\bar{f}(\boldsymbol{x}) = \int_D G(\boldsymbol{x} - \boldsymbol{x}')\, f(\boldsymbol{x}')\, \mathrm{d}\boldsymbol{x}' \tag{1}$$

where f is a turbulent field, G is some spatial filter (usually a sharp cutoff defined in Fourier space) of width equal to the grid spacing, and D is the flow domain.

Received Jan. 5, 1995; presented as Paper 95-0355 at the AIAA 33rd Aerospace Sciences Meeting, Reno, NV, Jan. 11–14, 1995; revision received May 19, 1995; accepted for publication May 22, 1995.

*Graduate Assistant, School of Aeronautics and Astronautics. Member AIAA.
†Assistant Professor, School of Aeronautics and Astronautics. Member AIAA.

The resulting equations of motion are as follows:

$$\frac{\partial \bar{\rho}}{\partial t} + \frac{\partial}{\partial x_i}(\bar{\rho}\tilde{u}_i) = 0 \tag{2}$$

$$\frac{\partial}{\partial t}(\bar{\rho}\tilde{u}_i) + \frac{\partial}{\partial x_j}(\bar{\rho}\tilde{u}_i\tilde{u}_j) = \frac{\partial}{\partial x_j}(\bar{\sigma}_{ij}) - \frac{\partial}{\partial x_j}(\tau_{ij}) \tag{3}$$

$$C_v\frac{\partial}{\partial t}(\bar{\rho}\tilde{T}) + C_v\frac{\partial}{\partial x_i}(\bar{\rho}\tilde{T}\tilde{u}_i) = \bar{\sigma}_{ij}\frac{\partial \tilde{u}_i}{\partial x_j} + \frac{\partial}{\partial x_i}\left(\bar{k}\frac{\partial \tilde{T}}{\partial x_i}\right) - C_v\frac{\partial}{\partial x_i}(q_i) \tag{4}$$

where

$$\bar{\sigma}_{ij} = -\bar{p}\delta_{ij} + \bar{\mu}\left(\frac{\partial \tilde{u}_i}{\partial x_j} + \frac{\partial \tilde{u}_j}{\partial x_i} - \frac{2}{3}\frac{\partial \tilde{u}_k}{\partial x_k}\delta_{ij}\right) \tag{5}$$

represents the resolved-scale stress tensor. The effects of the small scales are present in these equations through the SGS stress tensor and the SGS heat flux,

$$\tau_{ij} = \bar{\rho}(\widetilde{u_i u_j} - \tilde{u}_i\tilde{u}_j) \tag{6}$$

$$q_i = \bar{\rho}(\widetilde{u_i T} - \tilde{u}_i\tilde{T}) \tag{7}$$

respectively, and require modeling. A tilde is used to denote Favre averages ($\tilde{f} = \overline{\rho f}/\bar{\rho}$). Also ρ is the density, T is the temperature, u_i is the velocity vector, and k is the thermal conductivity. The specific heats at constant volume C_v and at constant pressure C_p are assumed in this study to be constant. The large-scale molecular viscosity $\bar{\mu}$ is assumed to obey the power law $\bar{\mu}/\bar{\mu}_0 = (\tilde{T}/\tilde{T}_0)^{0.76}$, whereas the large-scale pressure $\bar{p}$ is obtained from the filtered equation of state $\bar{p} = \bar{\rho}R\tilde{T}$. The molecular Prandtl number Pr is assumed to be 0.7. Note, that in deriving Eqs. (2–4), the viscous, pressure-dilatation and conduction terms were approximated in a similar fashion as by Erlebacher et al.[8]

B. Dynamic Modeling of the Subgrid Scales

The SGS terms [Eqs. (6) and (7)] are modeled here using a compressible flow version of the dynamic SGS model of Germano et al.[1]: for details, see Refs. 2 and 3. The model involves three coefficients, C, C_I, and Pr_t. They are automatically adjusted, as time progresses, based on the resolved flowfield information with the aid of a second filter (test filter $\hat{G}$) that has a filter width coarser than the grid used to perform the computations.

A refinement to the Moin et al.[2] model has been proposed by Lilly.[3] The two versions differ only on the type of a contraction used to determine uniquely the model coefficients, as is described later in this section. Both versions were tested in simulations, and comparative results are presented in Sec. III.B. The results presented in other sections were obtained using the Lilly contraction.

The model parameterization for the SGS stress and the SGS heat flux is given by

$$\tau_{ij} - \tfrac{1}{3}\tau_{kk}\delta_{ij} = -2C\bar{\rho}\Delta^2|\tilde{S}|\left(\tilde{S}_{ij} - \tfrac{1}{3}\tilde{S}_{kk}\delta_{ij}\right) \tag{8}$$

$$\tau_{kk} = 2C_I\bar{\rho}\Delta^2|\tilde{S}|^2 \tag{9}$$

$$q_i = -\frac{\bar{\rho}C\Delta^2|\tilde{S}|}{Pr_t}\frac{\partial \tilde{T}}{\partial x_i} \tag{10}$$

where

$$\tilde{S}_{ij} = \frac{1}{2}\left(\frac{\partial \tilde{u}_i}{\partial x_j} + \frac{\partial \tilde{u}_j}{\partial x_i}\right), \qquad |\tilde{S}| = (2\tilde{S}_{ij}\tilde{S}_{ij})^{\frac{1}{2}}$$

$$\Delta = (\Delta x\Delta y\Delta z)^{\frac{1}{3}}$$

The model coefficients are computed from

$$C = \left\{\left(L_{ij} - \tfrac{1}{3}L_{kk}\delta_{ij}\right)A_{ij}\right\}/(M_{pq}A_{pq}) \tag{11}$$

$$C_I = (L_{kk})/(2\hat{\bar{\rho}}\,\hat{\Delta}^2|\hat{\tilde{S}}|^2 - 2\Delta^2\widehat{\bar{\rho}|\tilde{S}|^2}) \tag{12}$$

$$Pr_t = C(\langle N_i B_i\rangle/\langle -K_j B_j\rangle) \tag{13}$$

where $\hat{}$ denotes test-filtered quantities, $\hat{\Delta} = (\hat{\Delta}_1\hat{\Delta}_2\hat{\Delta}_3)^{1/3}$ ($\hat{\Delta}_i$ is the width of the test filter in the ith direction), $\langle\ \rangle$ denotes some kind of averaging procedure, and

$$L_{ij} = \widehat{\bar{\rho}\tilde{u}_i\tilde{u}_j} - (1/\hat{\bar{\rho}})\widehat{\bar{\rho}\tilde{u}_i}\,\widehat{\bar{\rho}\tilde{u}_j} \tag{14}$$

$$M_{ij} = -2\hat{\Delta}^2\hat{\bar{\rho}}|\hat{\tilde{S}}|\left(\hat{\tilde{S}}_{ij} - \tfrac{1}{3}\hat{\tilde{S}}_{kk}\delta_{ij}\right) + 2\Delta^2\widehat{\bar{\rho}|\tilde{S}|\left(\tilde{S}_{ij} - \tfrac{1}{3}\tilde{S}_{kk}\delta_{ij}\right)} \tag{15}$$

$$N_i = \hat{\Delta}^2\hat{\bar{\rho}}|\hat{\tilde{S}}|\frac{\partial \hat{\tilde{T}}}{\partial x_i} - \Delta^2\widehat{\bar{\rho}|\tilde{S}|\frac{\partial \tilde{T}}{\partial x_i}} \tag{16}$$

$$K_i = \widehat{\bar{\rho}\tilde{u}_i\tilde{T}} - \left(1/\hat{\bar{\rho}}\right)\widehat{\bar{\rho}\tilde{u}_i}\,\widehat{\bar{\rho}\tilde{T}} \tag{17}$$

Finally, depending on the choice of contraction used,

$$A_{ij} = \begin{cases} \tilde{S}_{ij}: & \text{Moin's version} \\ M_{ij}: & \text{Lilly's version} \end{cases} \tag{18}$$

and

$$B_i = \begin{cases} \dfrac{\partial \tilde{T}}{\partial x_i}: & \text{Moin's version} \\ N_i: & \text{Lilly's version} \end{cases} \tag{19}$$

The model requires the above averaging procedure, an ad hoc solution,[1] to prevent numerical instabilities due to a simplification made in the derivation of the expressions for the model coefficients. For flows having a direction of homogeneity, spatial averaging is usually performed along that direction. For the case of homogeneous turbulence, this results in volume averaging and is the approach taken in this study. For this type of flow, the model coefficients vary only with time.

C. Computer Implementation

The numerical method for the direct and large eddy simulations employed a pseudo-spectral Fourier collocation scheme for spatial differencing and a third-order Runge–Kutta method for advancing in time.[9] The validity of the numerical implementation of the dynamic model was established by performing a priori tests similar to those by Moin et al.[2] and comparing with their reported data.

III. Results

A. Capturing of Compressibility Effects

The ability of the dynamic model to capture compressibility effects was examined by performing LES of decaying isotropic turbulence and comparing with the results obtained from DNS. A number of simulations were conducted at different initial levels of compressibility and Reynolds numbers. The cases listed in Table 1 were considered.

The level of compressibility of the initial fields was controlled by either varying the initial turbulent Mach number M_t (cases 1–3), or the fraction of the turbulent kinetic energy initially contained in the dilatational velocity field χ (cases 4–6). The effect of the turbulent Reynolds number Re_T on compressibility was examined in cases 7, 8, and 3 and also in cases 4, 2, and 9. [Here, $M_t = q/c$, $\chi = \langle q'^2/q\rangle^2$, and $Re_T = \rho q^4/(\epsilon\mu)$, where q is the rms magnitude of the fluctuation velocity, c is the mean speed of sound, q'^2 is the

Table 1 Case parameters

Case	M_t	χ	Re_T
1	0.2	0	2742
2	0.4	0	2742
3	0.6	0	2742
4	0.4	0	2157
5	0.4	0.1	2157
6	0.4	0.2	2157
7	0.6	0	735
8	0.6	0	2156
9	0.4	0	6170

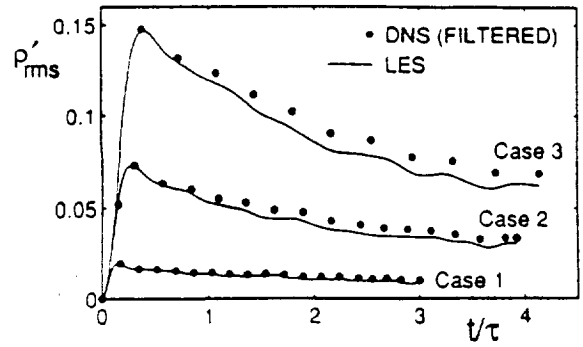

Fig. 1 Time evolutions of rms density fluctuations for cases 1–3; effects of initial M_t.

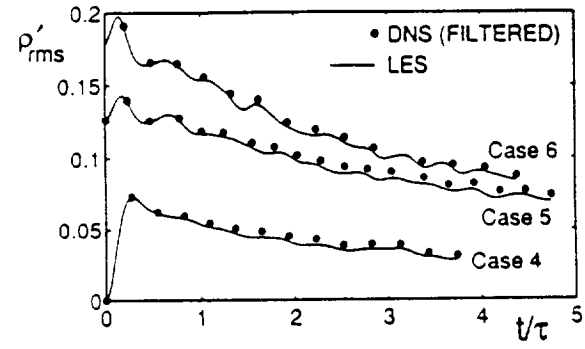

Fig. 2 Time evolutions of rms density fluctuations for cases 4–6; effects of initial χ.

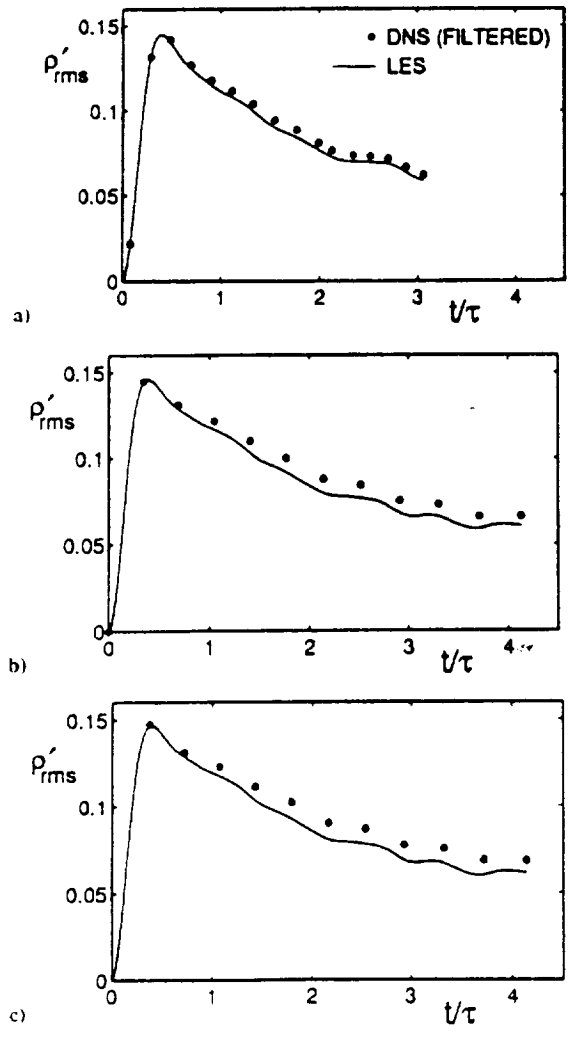

Fig. 3 Time evolutions of rms density fluctuations showing effects of initial Re_T for cases a) 7, b) 8, and c) 3.

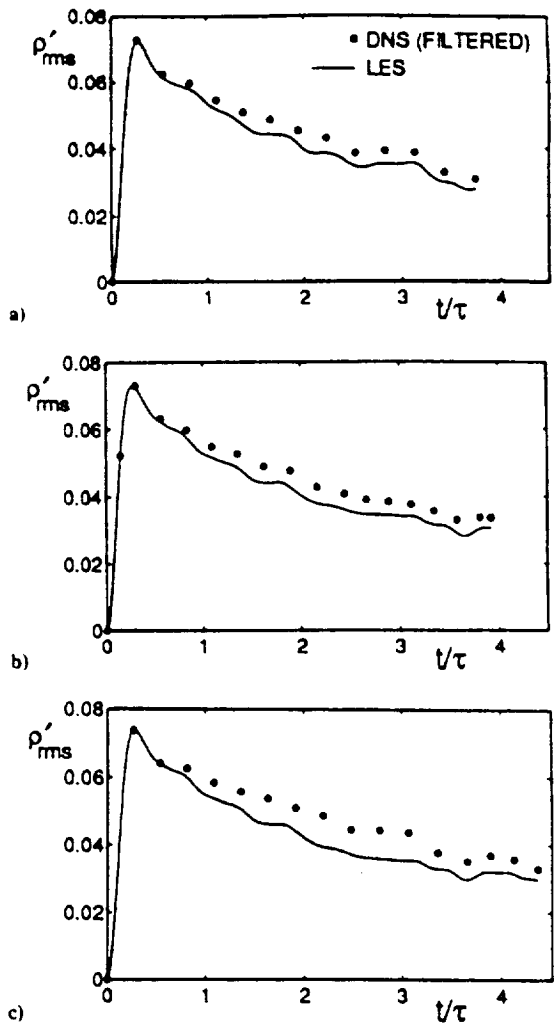

Fig. 4 Time evolutions of rms density fluctuations showing effects of initial Re_T for cases a) 4, b) 2, and c) 9.

rms magnitude of the dilatational fluctuation velocity, and ϵ is the dissipation rate of turbulent kinetic energy per unit mass.]

All cases with purely solenoidal initial velocity fields ($\chi = 0$) had uniform initial density and temperature fields, whereas the density and temperature fluctuations in the others were obtained from the isentropic relations and the condition for acoustic equilibrium (see Sarkar et al.[10]). The initial three-dimensional energy spectrum for each case was of the form

$$E(k) \propto k^4 \exp\left[-2(k/k_p)^2\right] \tag{20}$$

where the wave number of the peak of the spectrum k_p was set at 4. The LES were computed on $(32)^3$ grids, whereas the DNS were computed on $(128)^3$ grids.

Good, and percentwise consistent, agreement in all statistics considered was found between the LES and the DNS for all cases. This is shown, for example, in Figs. 1–4, where the evolutions of the rms density fluctuations between the LES and the (filtered) DNS data for the above sets of cases are compared. (The time axes in these figures have been scaled with the initial eddy turnover time τ, defined as the ratio of the lateral Taylor microscale and the rms fluctuation velocity in a direction.) Similar findings were obtained by comparing other statistical quantities, as well as one- and three-dimensional spectra, indicating that the dynamic SGS model seems to be capturing compressibility effects well for isotropic turbulence.

B. Comparison of Two Model Versions

In the preceding results, Lilly's version[3] of the dynamic model was employed. The Moin et al.[2] version was also tested for all cases. It predicted higher values for coefficient C_s, smaller values for coefficient C_t, and similar values with Lilly's version for Pr_t,

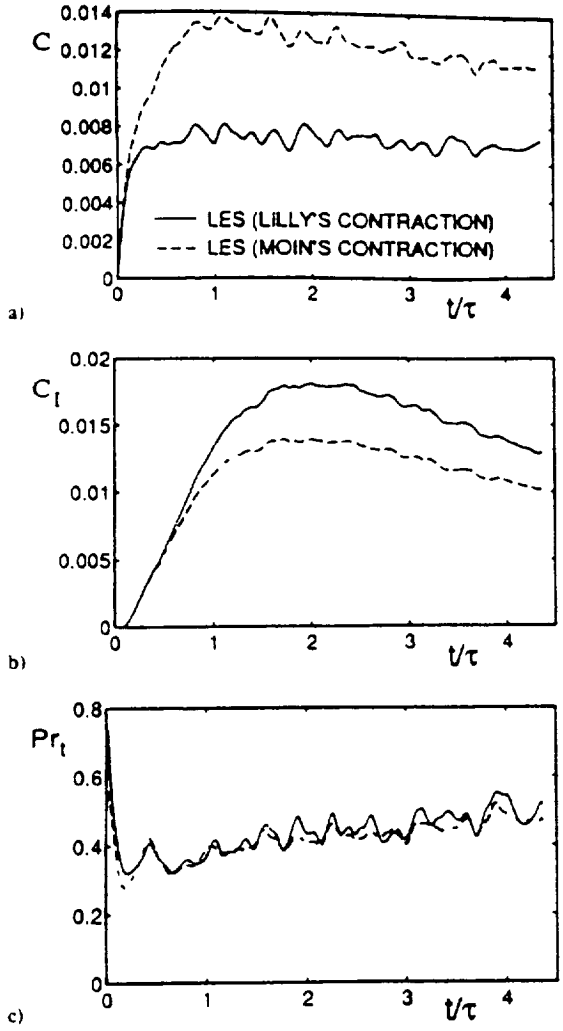

Fig. 5 Time evolutions of model coefficients showing effects of different contractions for case 6: a) C, b) C_l, and c) Pr_t.

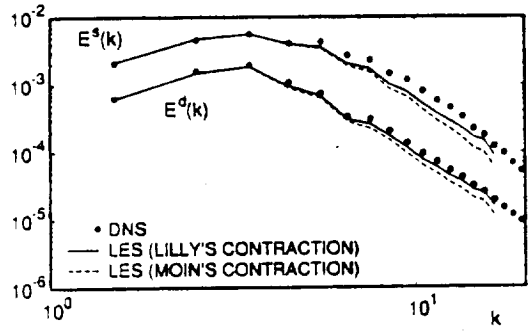

Fig. 6[a] Three-dimensional solenoidal and dilatational energy spectra for case 6 at $t/\tau = 4.37$; effects of different contractions.

as is shown, for case 6, in Fig. 5. Overall, the Moin et al. model also performed well but provided higher amounts of dissipation than Lilly's, as can be seen in the three-dimensional solenoidal and dilatational energy spectra for the same case shown in Fig. 6. This is most evident at higher wave numbers. The results are taken at a time when the turbulent kinetic energy had decayed to one-fourth of its initial value.

It should be noted that the values of Pr_t obtained from either version of the dynamic model were about 0.4–0.6 when the initial temperature field had a three-dimensional spectrum similar to the velocity's. In contrast, when the temperature was initially set to be uniform, Pr_t values higher than unity were predicted by the model. This behavior is believed to be due to differences in the initial transients of the temperature fields and is another indication for the need for dynamic modeling.

C. Effects of Varying the Test Filter Width

The only adjustable parameter in the dynamic model is the ratio $\alpha = \hat{\Delta}/\Delta$ of the widths of the test and the grid filter (see Sec. II.B). Based on a priori and a posteriori tests of incompressible transitional and turbulent channel flow, Germano et al.[1] suggested a value of 2 for future use. They also suggested further investigations using different types of flows. This value has since been adopted by other researchers and was used in most of the simulations presented here.

The sensitivity of the results on the choice of the filter width ratio was also examined here for two cases of highly compressible isotropic decaying turbulence (cases 6 and 9 from Table 1). Five values of α were considered: 1.6, 16/9, 2, 16/7, and 8/3. These correspond to Fourier cutoff wave numbers for the test filter of 10, 9, 8, 7, and 6, respectively. Note that the use of smaller or greater α values is undesirable, since it results in test-filtered quantities that are either almost unaffected by the filtering or contain only very large-scale information, respectively, and usually leads to ill-predicted model coefficients. Results for such cases are not presented here.

Noticeable differences in the evolutions of the model coefficients were found when different values for α were used in the simulations, as is shown for case 6 in Fig. 7. (The model coefficients were also calculated a priori from DNS results, and similar differences were seen.)

Surprisingly enough, the choice of α seems to have only a very small effect on the LES results.[1] For instance, the rms density fluctuations for case 6 (shown in Fig. 2 for $\alpha = 2$) varied by less than 3% for the five values of α considered (the differences are graphically indistinguishable). This difference was even smaller for case 9. Best agreement with the DNS was obtained when this parameter was set to 2.

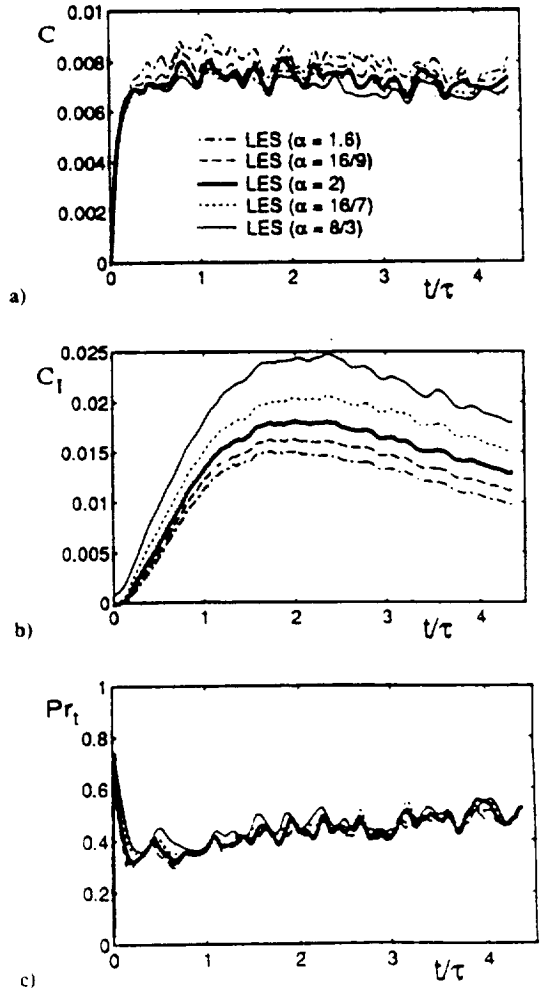

Fig. 7 Time evolutions of model coefficients showing effects of filter width ratio for case 6: a) C, b) C_l, and c) Pr_t.

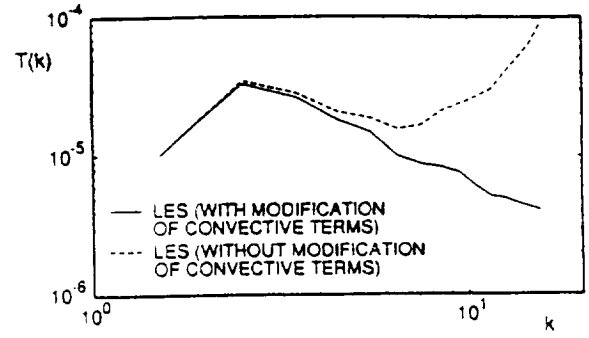

Fig. 8 Three-dimensional temperature spectra from simulations of the Comte-Bellot and Corrsin experiment; effects of modifying the convective terms.

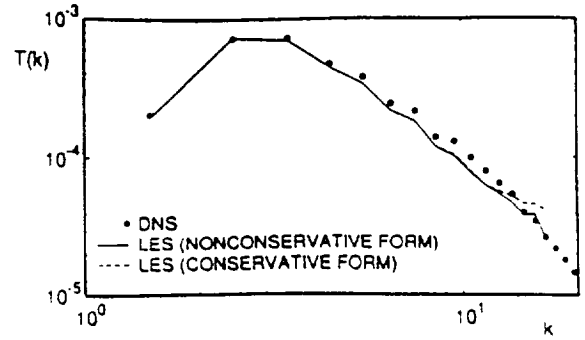

Fig. 9 Three-dimensional temperature spectra for case 6 at $t/\tau = 2.23$; effects of reformulating the energy equation.

D. Modification of the Convective Terms

It should be noted that the convective terms in the filtered momentum and filtered energy equations, Eqs. (3) and (4), were modified to the skew-symmetric form,

$$\frac{\partial}{\partial x_j}(f\tilde{u}_j) \rightarrow \frac{1}{2}\frac{\partial}{\partial x_j}(f\tilde{u}_j) + \frac{1}{2}\tilde{u}_j\frac{\partial f}{\partial x_j} + \frac{1}{2}f\frac{\partial \tilde{u}_j}{\partial x_j} \tag{21}$$

where f refers to $\bar{\rho}\tilde{u}_i$ and $\bar{\rho}\tilde{T}$, respectively.

This modification reduces the effect of aliasing errors,[11,12] which seems to be a bigger problem in LES than in DNS because the flowfields are less well resolved. Shown in Fig. 8 are three-dimensional temperature spectra from LES of the (high Reynolds number) Comte-Bellot and Corrsin experiment[13] (see Sec. III.F.2 for a description of the simulation). The LES without modifying the convective terms had a pile-up at high wave numbers, which led to instabilities, whereas the simulation with the modified terms was well behaved.

E. Alternative Formulation for the Energy Equation

In LES, there is also a choice in the formulation of the energy equation. The most popular approach is the solution of a nonconservative formulation (internal energy equation), since it requires only modeling of the SGS heat flux (see Sec. II.A). In contrast, if a conservative form (total energy equation) is used instead, then modeling of additional SGS terms is required. An alternative procedure, which does not require any additional modeling, is to solve for the pseudo total energy, defined as

$$\tilde{\phi} = \bar{\rho}C_v\tilde{T} + \bar{\rho}\tilde{u}_i\tilde{u}_i/2 \tag{22}$$

The resulting equation is

$$\frac{\partial}{\partial t}(\bar{\phi}) + \frac{\partial}{\partial x_i}(\tilde{\phi}\tilde{u}_i) = \frac{\partial}{\partial x_i}(\bar{\sigma}_{ij}\tilde{u}_j) - \tilde{u}_j\frac{\partial}{\partial x_i}(\tau_{ij}) + \frac{\partial}{\partial x_i}\left(\bar{k}\frac{\partial \tilde{T}}{\partial x_i}\right) - C_v\frac{\partial}{\partial x_i}(q_i) \tag{23}$$

This form is not in strong conservation law form; however, we refer to it here as the conservative form.

In LES of decaying compressible turbulence (case 6 from Table 1) both formulations performed well, but the nonconservative form was more accurate. The conservative form was found to have somewhat of a pileup in the high wave number part of the density and temperature spectra, as is shown in Fig. 9. This is believed to be due to aliasing errors originating from evaluating the temperature from the pseudo total energy.

F. Effects of Employing Different Spatial Test Filters

As was discussed in Sec. II.B, the dynamic model requires (test) filtering the resolved large-scale field. In flows that are homogeneous in at least two directions, the filtering can be performed efficiently (and exactly) in wave space using fast Fourier transforms. In more complex inhomogeneous flows, this is not possible, and some kind of discrete filtering has to be applied in physical space. In the next two sections, the formulation and testing of such filters is presented.

1. *Formulation of Spatial Filters*

Many different formulations of spatial filters were examined to determine their behavior in Fourier space. This was done because we believe it would be desirable for the spatial filter to have properties similar to the sharp cutoff filter.

For uniformly spaced grids, the spatial filters are formulated as follows:

$$\hat{f}_j + \sum_{n=1}^{N_i}\alpha_n\frac{\hat{f}_{j-n} + \hat{f}_{j+n}}{2} = \sum_{n=0}^{N_e-1}a_n\frac{f_{j-n} + f_{j+n}}{2} \tag{24}$$

where f_j is the function value at node j and $\hat{f}_j$ is the corresponding filtered function value. N_i is the number of implicit coefficients, which are given by $\{\alpha_n\}$, and N_e is the number of explicit coefficients, which are $\{a_n\}$.

The Fourier transform of the filtered function is given by $\hat{\mathcal{F}} = \mathcal{G}\mathcal{F}$, where $\mathcal{F}$ is the Fourier transform of the function and $\mathcal{G}$ is the filter transfer function. For the filter formulation (24), the filter transfer function is

$$\mathcal{G}_k = \left[\sum_{n=0}^{N_e-1}a_n\cos\left(\frac{2\pi kn}{N}\right)\right]\Bigg/\left[1 + \sum_{m=1}^{N_i}\alpha_m\cos\left(\frac{2\pi km}{N}\right)\right] \tag{25}$$

where k is the wavenumber and N is the number of grid points.

The first filters to be considered are approximations to the top-hat filter in physical space. The top-hat filter is defined by

$$\hat{G}(x - x') = \begin{cases} 1 & \text{if } x - \hat{\Delta}/2 \le x' \le x + \hat{\Delta}/2 \\ 0 & \text{otherwise} \end{cases} \tag{26}$$

where the filter width $\hat{\Delta}$ is assumed here equal to $2\Delta x$ (as was suggested in Sec. III.C). The convolution integral in Eq. (1) can be approximated in various ways. Using three collocation points and the trapezoid rule gives $a_0 = 1/2$ and $a_1 = 1/2$. With three collocation points one can improve the accuracy of the integration by using Simpson's rule, which gives $a_0 = 2/3$ and $a_1 = 1/3$. If the integration is done analytically, then a spectrally accurate formula is obtained.

The filter transfer functions for these schemes are shown in Fig. 10a against that of the sharp cutoff filter. The top-hat filter behaves very differently from the sharp cutoff filter and is more like the Gaussian filter in that some of the low wave number modes are reduced in amplitude whereas some of the high wave number modes are retained.

A second set of filters is obtained by approximating the sharp cutoff filter in a least squares sense, with certain constraints imposed. Three constraints are considered. Constraint 1 is that the filter be mean preserving. This is important because the filter is supposed to separate large and small scales and should not alter a uniform field. For the filter to be mean preserving, it is necessary that $\mathcal{G}(0) = 1$. Constraint 2 is that the end point of the filter transfer function is fixed to be zero; i.e., $\mathcal{G}(k = N/2) = 0$. This constraint is not required on any physical basis; however, we believe it is a desirable property of the filter transfer function. Constraint 3 is that the ratio of the

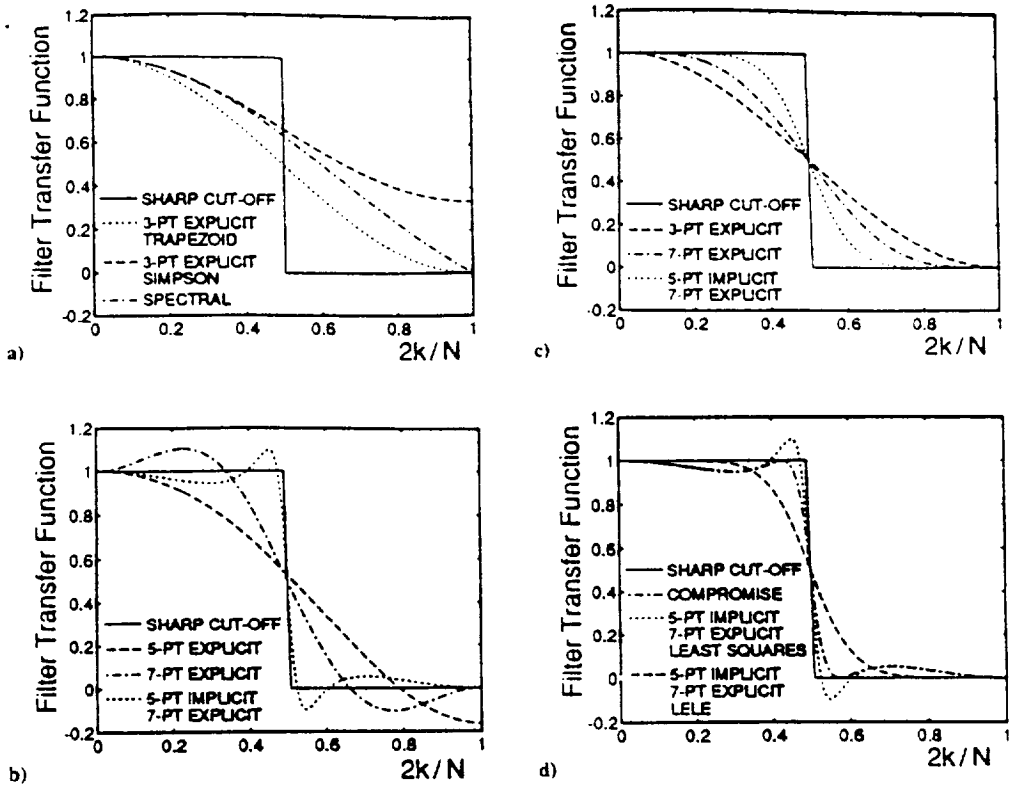

Fig. 10 Comparison of filter transfer functions for various spatial filters: a) top-hat filters, b) sharp cutoff least squares filters, c) Lele filters, and d) compromise filter.

filter width to the grid spacing, $\hat{\Delta}/\Delta x$, be 2, since this is the chosen standard value.

To implement constraint 3, one has to define the filter width for a given filter. We have chosen to define the filter width in a manner analogous to how the integral length scale is defined for a two-point correlation. For a discrete filter this corresponds to

$$\hat{\Delta} = \sum_{j=1}^{N} \frac{\hat{G}_j}{\hat{G}_1} \Delta x \tag{27}$$

Since the filters are mean preserving

$$\sum_{j=1}^{N} \hat{G}_j = \mathcal{G}_0 = 1 \tag{28}$$

and

$$\frac{\hat{\Delta}}{\Delta x} = \frac{1}{\hat{G}_1} = 1 \Big/ \frac{1}{N} \sum_{k=-N/2+1}^{N/2} \mathcal{G}_k \tag{29}$$

This definition is dependent on the number of grid points N, which is undesirable. A more useful formulation can be obtained by letting $k' = 2k/N$, $\Delta k' = 2\Delta k/N$ (where $\Delta k = 1$) and $\mathcal{G}'(k') = \mathcal{G}(k)$, where $\mathcal{G}(k)$ is given by Eq. (25), so that

$$\frac{\hat{\Delta}}{\Delta x} = 1 \Big/ \frac{1}{2} \sum_{k=-N/2+1}^{N/2} \mathcal{G}'(k')\, \Delta k' \tag{30}$$

Taking the limit $N \to \infty$ and using the symmetry of $\mathcal{G}'$ results in

$$\frac{\hat{\Delta}}{\Delta x} = 1 \Big/ \int_0^1 \mathcal{G}'(k')\, \mathrm{d}k' \tag{31}$$

This definition is consistent with the length scale obtained from the cutoff wave number when a sharp cutoff filter is used, which is the reason it was chosen. An alternate definition in terms of the second moment of the filter function was used by Leonard[14] for the top-hat filter and the Gaussian filter; however, for the sharp cutoff filter such a definition gives an infinite filter width, and for some of the other filters considered in this study, an imaginary filter width is obtained. Therefore, the definition given in Eq. (31) was adopted.

The least squares problem is formulated as minimizing the integrated square difference between the filter transfer function $\mathcal{G}'(k')$ and the transfer function for the sharp cutoff filter $\mathcal{G}'_{sco}(k')$. The free parameters are the filter coefficients $\{a_n\}$ and $\{\alpha_m\}$. From constraint 1 we have

$$\mathcal{G}'(0) = \left[\sum_{n=0}^{N_a-1} a_n \Big/ \left(1 + \sum_{m=1}^{N_\alpha} \alpha_m \right) \right] = 1 \tag{32}$$

Constraint 2 gives

$$\mathcal{G}'(k' = 1) = 0 = \sum_{n=0}^{N_a-1} a_n \tag{33}$$

These two equations can be solved for a_{N_a-1} and a_{N_a-2} in terms of the other parameters, so that the numbers of degrees of freedom is reduced by two. Constraint 3 was enforced by using a penalty function. The function to be minimized is

$$E = \int_0^1 [\mathcal{G}'(k') - \mathcal{G}'_{sco}(k')]^2\, \mathrm{d}k' + A \left(\frac{\hat{\Delta}}{\Delta x} - 2 \right)^2 \tag{34}$$

The Nelder–Mead simplex search algorithm[15] was implemented to solve the minimization problem. The integrals needed to evaluate E were calculated using Romberg integration with the error tolerance set to 10^{-14}. The constant A was set to 10^{10} so that constraint 3 was met with an error on the order of 10^{-6}. For explicit filters, the integrals can be evaluated analytically, and the minimization problem can be solved exactly. This was used as a check of the numerical procedure. For this case, Eq. (31) reduces to

$$\hat{\Delta}/\Delta x = 1/a_0 \tag{35}$$

Table 2 Summary of spatial filters tested in simulations

Filter	a_0	a_1	a_2	a_3	α_1	α_2
1 3-pt explicit, trapezoid	0.5	0.5				
2 3-pt explicit, Simpson	0.6666667	0.3333333				
3 5-pt explicit, least squares	0.4726761	0.5819719	−0.05464480			
4 7-pt explicit, least squares	0.5	0.6744132	0	−0.1744132		
5 5-pt implicit–7-pt explicit, least squares	0.5	0.8105146	0.4830535	0.1725389	0	0.9661071
6 5-pt implicit–7-pt explicit, Lele	0.5	0.75	0.3	0.05	0	0.6
7 5-pt implicit–7-pt explicit, compromise	0.5	0.8056734	0.4684092	0.1627358	0	0.9368185

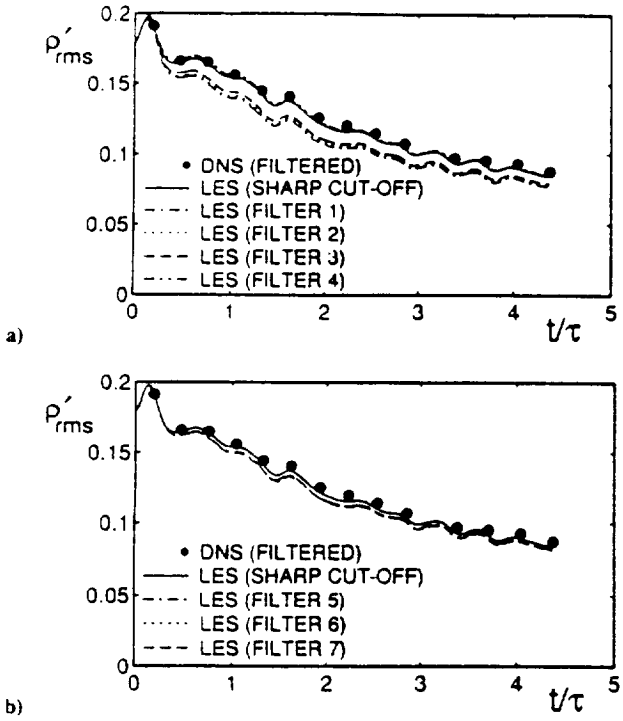

Fig. 11 Time evolutions of rms density fluctuations for case 6; effects of spatial filters: a) explicit and b) implicit.

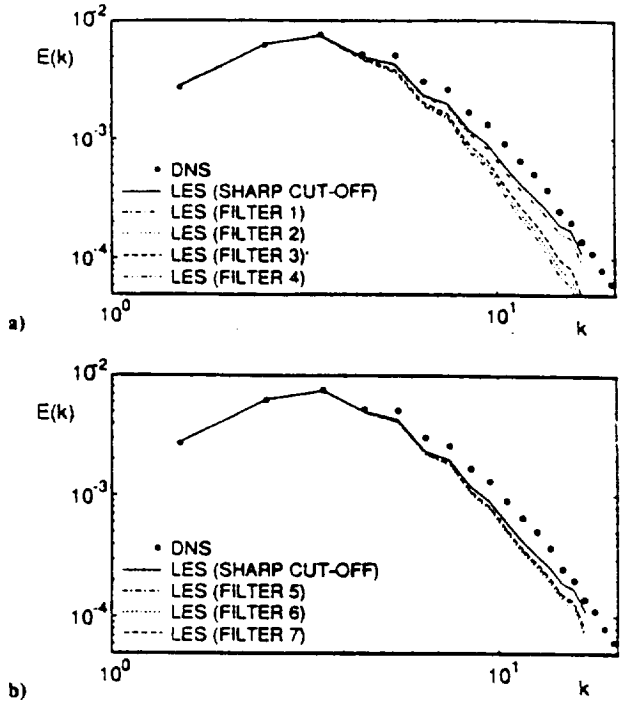

Fig. 12 Three-dimensional energy spectra for case 6 at $t/\tau = 4.37$; effects of spatial filters: a) explicit and b) implicit.

The resulting filter coefficients are given in Table 2. The three-point explicit filter is the same as the trapezoid filter. No five-point explicit filter was found that met all of the constraints, and so constraints 2 and 3 were dropped for the five-point explicit filter shown. The highest order explicit filter considered is a seven-point filter. A number of implicit filters were found. The one discussed here is a five-point implicit–seven-point explicit filter.

The least squares filters are compared to the sharp cutoff filter in Fig. 10b. As the number of filter coefficients is increased, better agreement with the sharp cutoff filter is obtained, as expected. However, the filter transfer functions are oscillatory and display large amplitude overshoots, which is believed to be undesirable.

A third set of filters is obtained following Lele[16] in which a different set of constraints are placed on the filter transfer function. To compare these filters to the sharp cutoff filter with $\tilde{\Delta}/\Delta x = 2$, the extra constraint $\mathcal{G}(k = N/4) = 1/2$ was imposed. The filters obtained are shown in Fig. 10c. In general, the filters are smooth, monotonically decreasing from 1 to 0. However, the filters are not as sharp as the five-point implicit method obtained from the least squares approach. Note that the three-point explicit filter is the same as the trapezoid filter.

The filters obtained from Lele's formulation are very smooth, whereas the filters found from the least squares approach are much sharper but exhibit oscillations. In an attempt to reach a compromise between the two filters, we constructed filters obtained by combining the filter coefficients in the following way:

$$a_n = \psi a_n^{ls} + (1-\psi)a_n^{Lele}, \qquad \alpha_n = \psi \alpha_n^{ls} + (1-\psi)\alpha_n^{Lele} \quad (36)$$

Figure 10d shows the transfer function for the five-point implicit–seven-point explicit filter with $\psi = 0.92$. This compromise filter gives a transfer function that is sharper than that from the Lele formulation but does not have as large an overshoot as that from the least squares approach.

2. *Testing of Spatial Filters*

A number of spatial filters from the preceding section were tested in simulations. The filters considered are shown in Table 2 (see also Fig. 10). Homogeneous flow test cases were chosen, so that the effects of these filters can be compared to that of the sharp cutoff filter, defined in wave space, as well as against available DNS or experimental data.

Results from simulations of a highly compressible decaying isotropic flow (case 6 from Table 1) are presented first. The histories of the rms density fluctuations are compared in Fig. 11. Figure 12 shows comparisons of three-dimensional energy spectra taken at a time when the turbulent kinetic energy had decayed to one-fourth of its initial value. The results from a DNS are also included in these figures for further comparison. The evolutions of the model coefficient C are shown in Fig. 13. All spatial filters are found to be more dissipative at higher modes than the sharp cutoff. All implicit filters performed well and, among them, filter 7 was found to be the best candidate. Most of the explicit filters were very dissipative and performed poorly, with the exception of filter 4 which gave results very similar to those from the sharp cutoff filter. However, this filter predicted small negative values for the coefficient C_I and, consequently, from Eq. (9), negative values for the subgrid-scale turbulent kinetic energy τ_{ii}. This may, in some cases, lead to numerical instabilities, although it did not here.

The spatial filters were also tested for the case of a nearly incompressible turbulence. The isotropic grid-generated (high Reynolds

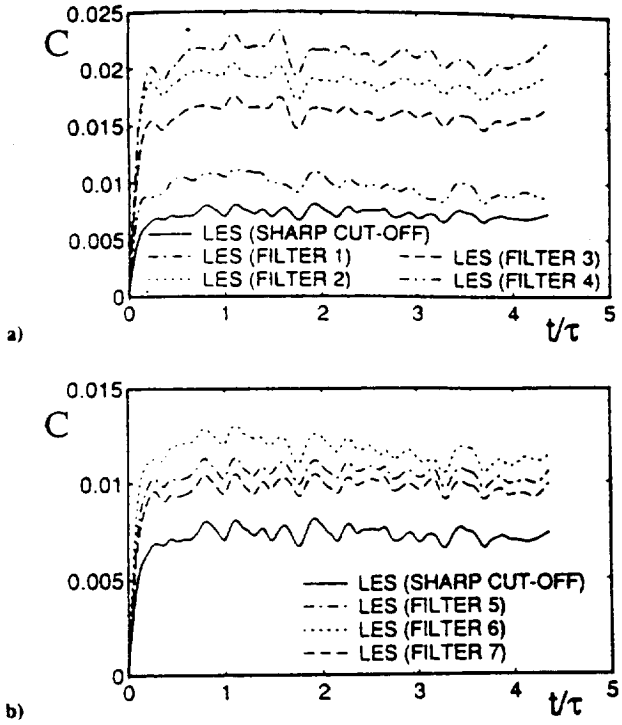

Fig. 13 Time evolution of model coefficient C for case 6; effects of spatial filters: a) explicit and b) implicit.

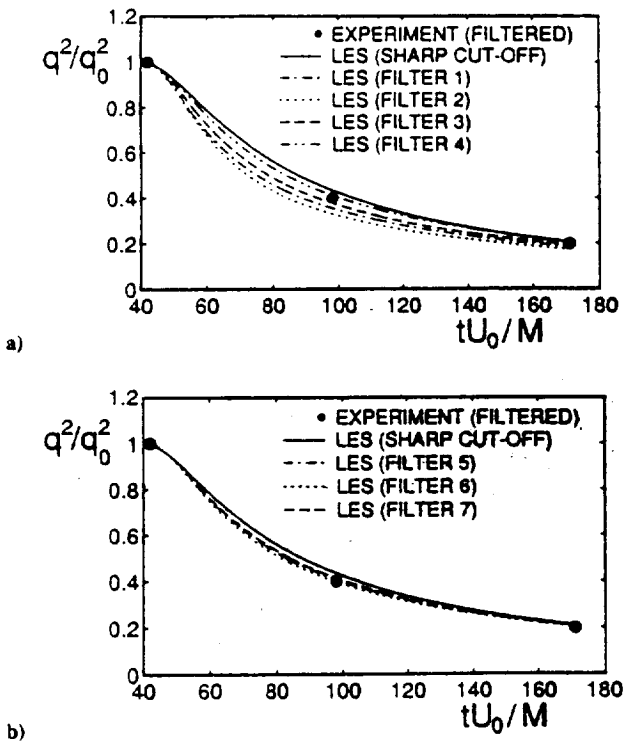

Fig. 14 Time evolution of turbulent kinetic energy from simulations of Comte-Bellot and Corrsin's experiment; effects of spatial filters: a) explicit and b) implicit.

number) turbulence experiment of Comte-Bellot and Corrsin[13] was simulated as a temporal decay on a $(32)^3$ grid. The initial velocity fields for the simulations were purely solenoidal and designed to have the same three-dimensional spectrum as that reported at $tU_0/M = 42$ in the experiment (where U_0 is the mean flow velocity and M is the grid size). The initial pressure fields were computed from the incompressible Poisson equation, while the density was assumed to be uniform. The initial Mach number was set to 0.3.

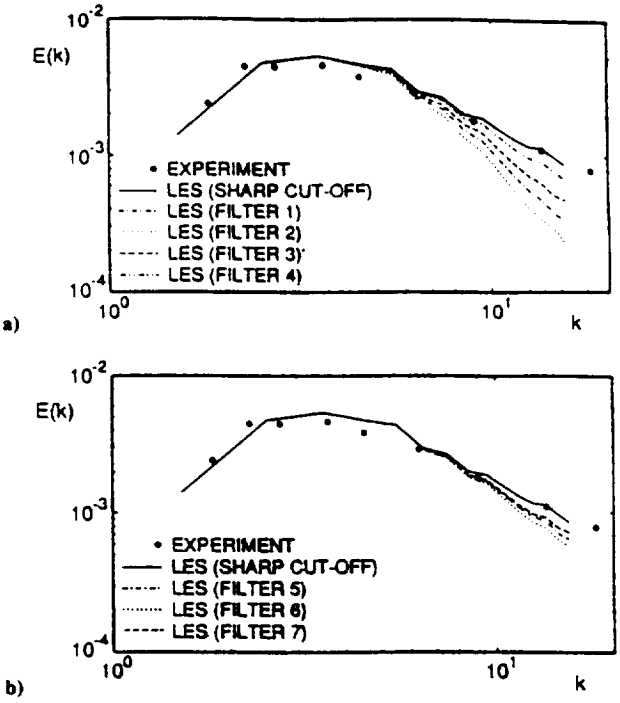

Fig. 15 Three-dimensional energy spectra from simulations of Comte-Bellot and Corrsin's experiment at $tU_0/M = 98$; effects of spatial filters: a) explicit and b) implicit.

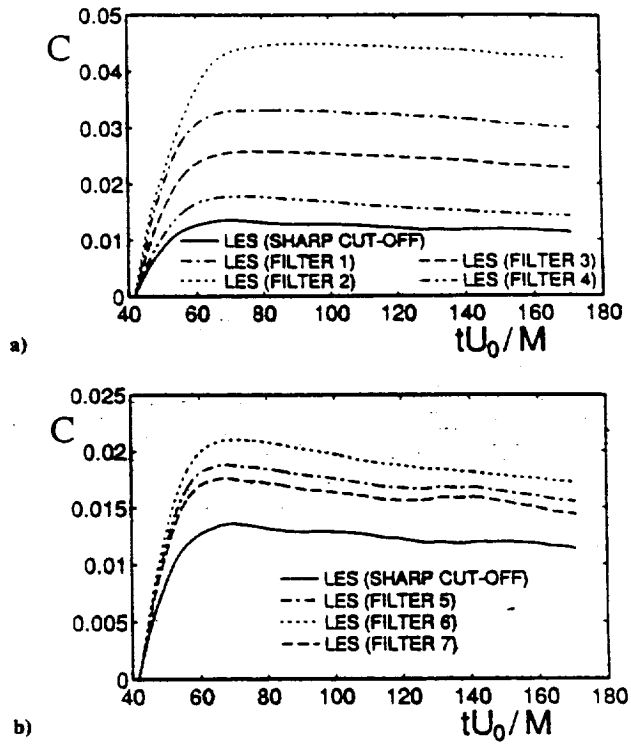

Fig. 16 Time evolution of model coefficient C from simulations of Comte-Bellot and Corrsin's experiment; effects of spatial filters: a) explicit and b) implicit.

The sharp cutoff filter was employed first in the dynamic model. The predicted time development of the turbulent kinetic energy and the three-dimensional energy spectra compare well with the available experimental data, as shown in Figs. 14 and 15, respectively.

The performance of the spatial filters was then examined. Figures 14 and 15 also present results from these simulations. The evolution of the model coefficient C predicted from the various spatial filters are compared against the one from the sharp cutoff filter in Fig. 16. Filter 6 was found to be the most dissipative of the implicit

filters. However, all of these filters performed well and similarly to the sharp cutoff filter. Filter 4, the seven-point explicit filter, again performed very well, in contrast to the three-point and five-point explicit filters, which provided great amounts of dissipation.

For the Comte-Bellot and Corrsin simulation, we neglected C_I on the basis that for nearly-incompressible flows τ_{kk} is small compared to the thermodynamic pressure.[8,17,18] This was done to avoid instabilities in the computations that occurred during the initial transient period for some of the spatial filters. However, negligible difference on the results was observed when the sharp cutoff filter was used and C_I was computed from the dynamic model.

IV. Conclusions

Several issues involving the use of the dynamic SGS model in performing LES of compressible turbulent flows have been examined by employing the model in simulations and comparing with results from DNS or experiments. Decaying isotropic turbulence was considered in order to evaluate the performance of the model separately from the effects of inhomogeneity.

We conducted a parametric study where the levels of compressibility of the initial flow fields were varied. The model, with its ability to adjust itself to the flow conditions, was found to predict well, from a statistical viewpoint, the bulk of the flow. The dynamic model was able to capture compressibility effects well and does not require any explicit compressibility corrections.

In performing LES of inhomogeneous compressible turbulent flows using the dynamic model, the filtering operation required by the model can not be done in wave space but, rather, has to be approximated in physical space. We have examined the behavior of several implicit and explicit spatial filters in wave space. We also conducted simulations of highly compressible and high Reynolds number nearly incompressible cases of decaying isotropic turbulence to study the performance of such filters against that of the sharp cutoff filter defined conveniently in Fourier space. The five-point implicit–seven-point explicit filters examined performed extremely well and should be considered as good candidates for future use. However these filters would be more expensive to employ than explicit ones. The former filters have transfer functions that are much sharper than the other filters near the cutoff mode, but exhibit oscillations that as suggested by the simulations are not of serious concern. The seven-point explicit filter gave good results also; however, it predicted small negative values for model coefficient C_I, which is undesirable. The three-point and five-point explicit filters were very dissipative, especially in the high Reynolds number simulation.

Two versions of the dynamic model were employed and tested in LES. The version by Lilly[3] was found to be more accurate than the version by Moin et al.[2]

A number of simulations were also performed to study the effect of the filter width ratio—the only adjustable parameter in the dynamic model. The results suggest a great insensitivity of the model to this parameter. Best agreement with the results from DNS was obtained when this parameter was set to 2.

Modification of the convective terms in the filtered momentum and filtered energy equations improves the accuracy of the simulations, as well as the stability of the numerical method. In addition, the nonconservative formulation of the energy equation was found to be somewhat better than the conservative form.

Acknowledgments

This work was supported by NASA Langley under Grant NAG-1-1509. Computer resources were provided by the National Academy of Sciences and Purdue University. The authors would like to thank Thomas Lund and Ugo Piomelli for their helpful suggestions concerning this work.

References

[1]Germano, M., Piomelli, U., Moin, P., and Cabot, W., "A Dynamic Subgrid-scale Eddy-viscosity Model," *Physics of Fluids A*, Vol. 3, July 1991, pp. 1760–1765.

[2]Moin, P., Squires, K., Cabot, W., and Lee, S., "A Dynamic Subgrid-scale Model for Compressible Turbulence and Scalar Transport," *Physics of Fluids A*, Vol. 3, Nov. 1991, pp. 2746–2757.

[3]Lilly, D. K., "A Proposed Modification of the Germano Subgrid-scale Closure Method," *Physics of Fluids A*, Vol. 4, March 1992, pp. 633–635.

[4]Wong, V. C., "A Proposed Statistical-dynamic Closure Method for the Linear or Nonlinear Subgrid-scale Stresses," *Physics of Fluids A*, Vol. 5, May 1992, pp. 1080–1082.

[5]Ghosal, S., Lund, T. S., and Moin, P., "A Local Dynamic Model for Large Eddy Simulation," *Annual Research Briefs-1992*, Center for Turbulence Research, Stanford Univ., Stanford, CA, 1992, pp. 3–25.

[6]Piomelli, U., and Liu, J., "Large Eddy Simulation of Rotating Channel Flows Using a Localized Dynamic Model," *74th AGARD/FDP Symposium on Application of Direct and Large Eddy Simulation to Transition and Turbulence*, AGARD-CP-551, 3.1–3.9, Chania, Greece, 1994.

[7]El Hady, N. M., Zang, T. A., and Piomelli, U., "Applications of the Dynamic Subgrid-scale Model to Axisymmetric Transitional Boundary Layer at High Speed," *Physics of Fluids A*, Vol. 6, March 1994, pp. 1299–1309.

[8]Erlebacher, G., Hussaini, M. Y., Speziale, C. G., and Zang, T. A., "Toward the Large-eddy Simulation of Compressible Turbulent Flows," *Journal of Fluid Mechanics*, Vol. 238, May 1992, pp. 155–185.

[9]Blaisdell, G. A., Mansour, N. N., and Reynolds, W. C., "Compressibility Effects on the Growth and Structure of Homogeneous Turbulent Shear Flow," *Journal of Fluid Mechanics*, Vol. 256, Nov. 1993, pp. 443–485.

[10]Sarkar, S., Erlebacher, G., Hussaini, M. Y., and Kreiss, H. O., "The Analysis and Modeling of Dilatational Terms in Compressible Turbulence," *Journal of Fluid Mechanics*, Vol. 227, June 1991, pp. 473–493.

[11]Zang, T. A., "On the Rotational and Skew-symmetric Forms for Incompressible Flow Simulations," *Applied Numerical Mathematics*, Vol. 7, Jan. 1991, pp. 27–40.

[12]Blaisdell, G. A., Spyropoulos, E. T., and Qin, J. H., "The Effect of the Formulation of Nonlinear Terms on Aliasing Errors in Spectral Methods," *Applied Numerical Mathematics* (submitted for publication).

[13]Comte-Bellot, G., and Corrsin, S., "Simple Eulerian Time Correlation of Full and Narrow Band Velocity Signals in Grid Generated, Isotropic Turbulence," *Journal of Fluid Mechanics*, Vol. 48, July 1971, pp. 273–337.

[14]Leonard, A., "On the Energy Cascade in Large-eddy Simulations of Turbulent Fluid Flows," *Advances in Geophysics*, Vol. 18A, 1974, pp. 237–248.

[15]Press, W. H., Flannery, B. P., Teukolsky, S. A., and Vetterling, W. T., *Numerical Recipes: The Art of Scientific Computing*, Cambridge Univ. Press, Cambridge, England, UK, 1986, p. 289.

[16]Lele, S. K., "Compact Finite Difference Schemes with Spectral-like Resolution," *Journal of Computational Physics*, Vol. 103, Nov. 1992, pp. 16–42.

[17]Zang, T. A., Dahlburg, R. B., and Dahlburg, J. P., "Direct and Large Eddy Simulations of Three-Dimensional Compressible Navier–Stokes Turbulence," *Physics of Fluids A*, Vol. 4, Jan. 1992, pp. 127–140.

[18]Sreedhar, M., and Ragab, S., "Large Eddy Simulation of Longitudinal Stationary Vortices," *Physics of Fluids A*, Vol. 6, July 1994, pp. 2501–2514.

Attachment B

ELSEVIER

Applied Numerical Mathematics 20 (1996) 1–13

APPLIED NUMERICAL MATHEMATICS

The effect of the formulation of nonlinear terms on aliasing errors in spectral methods

G.A. Blaisdell *, E.T. Spyropoulos, J.H. Qin

School of Aeronautics and Astronautics, Purdue University, West Lafayette, IN 47907-1282, USA

Abstract

The effect on aliasing errors of the formulation of nonlinear terms, such as the convective terms in the Navier–Stokes equations of fluid dynamics, is examined. A Fourier analysis shows that the skew-symmetric form of the convective term results in a reduced amplitude of the aliasing errors relative to the conservative and nonconservative forms. The three formulations of the convective term are tested for Burgers' equation and in large-eddy simulations of decaying compressible isotropic turbulence. The results for Burgers' equation show that, while in certain cases the nonconservative form has the lowest error, the skew-symmetric form is the most robust. For the turbulence simulations, the skew-symmetric form gives the most accurate results, consistent with the error analysis.

1. Introduction

Numerical simulation of nonlinear conservation laws, such as the Navier–Stokes equations of fluid dynamics, can give rise to nonlinear instabilities. This was pointed out long ago by Philips [14]. The instability was attributed to aliasing errors, in which the product of low order modes creates high frequency modes that when discretized appear as low frequency modes. This difficulty was overcome by Arakawa [2] for two-dimensional, incompressible problems using the vorticity-streamfunction formulation by developing a finite differencing scheme which satisfies certain global conservation properties. The modifications ensure conservation of kinetic energy and squared vorticity in the absence of external and viscous forces and time differencing errors. It was found that by meeting these constraints the instability was suppressed.

This idea was extended to three dimensional simulations by Kwak [11], who used primitive variables and rewrote the convective term in the momentum equation,

$$u_j \frac{\partial u_i}{\partial x_j}, \tag{1.1}$$

* Corresponding author.

SSDI 0168-9274(96)00005-0

in the modified form

$$\frac{1}{2}\frac{\partial}{\partial x_j}\left(u_i u_j\right) + \frac{1}{2}u_j\frac{\partial u_i}{\partial x_j}, \tag{1.2}$$

where use has been made of the conservation of mass equation for incompressible flow, $\partial u_j/\partial x_j = 0$. The formulations in (1.1) and (1.2) are referred to as the nonconservative and skew-symmetric formulations respectively. A third formulation is the conservative form,

$$\frac{\partial}{\partial x_j}\left(u_i u_j\right). \tag{1.3}$$

Using the skew-symmetric formulation in (1.2), Kwak showed that the integral conservation properties are maintained by the finite differencing scheme. Mansour, Moin, Reynolds and Ferziger [12] showed that the identity equating (1.1) and (1.2) does not hold numerically and that this is the reason the the global conservation properties are not satisfied. One can show that the reason (1.1) is not equivalent to (1.2) numerically is the occurrence of aliasing errors. The skew-symmetric form of the convective terms were extended to the simulation of compressible flows in [4,8,15].

In [12] the rotational form of the convective term was considered. It is given by

$$u_j\left(\frac{\partial u_j}{\partial x_i} - \frac{\partial u_i}{\partial x_j}\right) - \frac{\partial}{\partial x_j}\left(\frac{1}{2}u_i u_j\right), \tag{1.4}$$

and is widely used in incompressible simulations. The rotational form ensures additional conservation properties including that of helicity [10]. Horiuti [10] performed numerical experiments of incompressible turbulent channel flow using a finite differencing scheme with the skew-symmetric form and the rotational form, and concluded that the skew-symmetric form was superior. Horiuti attributed the poor performance of the rotational form to large truncation errors in the vicinity of the wall. Zang [16] performed spectral calculations of incompressible turbulent channel flow using the skew-symmetric form and the rotational form of the convective terms. He was also able to perform dealiased simulations in which aliasing errors were removed, and he showed that the poor performance of the rotational form was due to aliasing errors.

Zang states that no theoretical analysis is available to explain why aliasing errors are reduced for the skew-symmetric form. In the current paper we examine the aliasing errors created by the nonlinear convective term and show, through a Fourier analysis, that the magnitude of the aliasing errors is reduced for the skew-symmetric form compared to conservative and nonconservative forms. The analysis method for the rotational form becomes too complicated to draw any conclusions regarding it; however, the low aliasing errors for the skew-symmetric form can be understood. We then test the three formulations on Burgers' equation and in large-eddy simulations of compressible isotropic turbulence.

There are other methods of reducing aliasing errors besides reformulating the convective terms. Orszag [13] pointed out that aliasing errors for a product can be eliminated by truncating the Fourier coefficients of the velocity and the product using the so-called "2/3 rule." For some problems, such as simulation of compressible turbulence, which are best time advanced in physical space rather than in Fourier space, this procedure requires additional Fourier transforms and can be prohibitively expensive. An alternative which does not use Fourier transforms is due to Anderson [1]. With this procedure the velocity and the product are filtered in physical space using a digital filter. Aliasing errors are eliminated by forming the product on a refined grid. This procedure can also be expensive

if high accuracy is required. Canuto et al. [5] point out that aliasing errors cease to be an issue if adequate resolution is used. However, for problems such as large-eddy simulation of high Reynolds number turbulence, in which the flow field is not well resolved, aliasing errors are important and increased resolution is not a possible solution. Therefore, the reformulation of the convective terms discussed in the current paper offers an alternative to more expensive dealiasing procedures.

2. Error analysis

We are interested in examining the aliasing errors that arise in using pseudospectral Fourier methods to solve nonlinear partial differential equations. The specific problem we are concerned with is the solution of the compressible Navier–Stokes equations, and so we take the nonlinear convective terms as the form of interest. In order to analyze the aliasing errors, we consider a model problem of evaluating a derivative of the form

$$\frac{\partial}{\partial x}(fg). \tag{2.1}$$

The convective terms in the momentum and energy equations (and in a passive scalar or chemical species equation) can be put in this form.

Consider the product fg. Using a spectral Fourier method, the functions f and g are represented by a finite set of Fourier modes evaluated at N discrete collocation points as follows

$$f_j = \sum_{n=-N/2+1}^{N/2} \widehat{f}_n e^{ik_n x_j}, \tag{2.2}$$

$$g_\ell = \sum_{m=-N/2+1}^{N/2} \widehat{g}_m e^{ik_m x_\ell}, \tag{2.3}$$

where $x_j = (j-1)L/N$, $(j = 1, \ldots, N)$, are the collocation points, $k_n = 2\pi n/L$ are the wavenumbers, L is the length of the computational domain, and $\widehat{f}_n$ and $\widehat{g}_m$ are the Fourier coefficients. The continuous functions $f(x)$ and $g(x)$ are approximated by a finite set of Fourier modes,

$$f(x) = \sum_{n=-N/2+1}^{N/2} \widehat{f}_n e^{ik_n x}, \tag{2.4}$$

$$g(x) = \sum_{m=-N/2+1}^{N/2} \widehat{g}_m e^{ik_m x}. \tag{2.5}$$

The product is

$$f(x)g(x) = \sum_{n=-N/2+1}^{N/2} \sum_{m=-N/2+1}^{N/2} \widehat{f}_n \widehat{g}_m e^{i(k_n+k_m)x}. \tag{2.6}$$

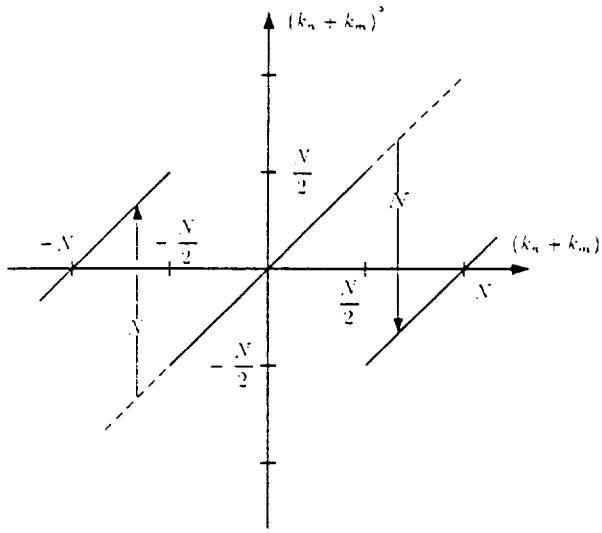

Fig. 1. Aliased wavenumber versus true wavenumber.

When this product is discretized, some modes will have values of $(k_n + k_m)$ which lie outside the range of resolved wavenumbers, which is given by

$$\left\{ -\frac{2\pi}{L}\left(\frac{N}{2}-1\right),\ldots,\frac{2\pi}{L}\left(\frac{N}{2}\right)\right\}$$

for N even. On the discrete collocation points these modes will be identical to modes that lie within the range of resolved wavenumbers. Thus the unresolved, high wavenumber modes are "aliased" to resolved, lower wavenumber modes. (See [5] for a more complete description.) A Fourier mode which has a wavenumber outside the resolved wavenumber range is aliased to the mode within the resolved wavenumber range which has a wavenumber that differs from $(k_n + k_m)$ by an integer multiple of $2\pi N/L$. We will denote the wavenumber of the resolved mode to which the mode $(k_n + k_m)$ is aliased by $(k_n + k_m)^\circ$. A graph of $(k_n + k_m)^\circ$ as a function of $(k_n + k_m)$ is shown in Fig. 1. Note that if $(k_n + k_m)$ lies within the range of resolved wavenumbers then the mode is not aliased to a lower frequency mode and $(k_n + k_m)^\circ = (k_n + k_m)$.

The discrete derivative is found by transforming the discrete product values, multiplying the Fourier coefficients by $\mathrm{i} = \sqrt{-1}$ times the wavenumber, and inverting the transform. This procedure gives

$$\left[\frac{\partial}{\partial x}(fg)\right]_j = \sum_{n=-N/2+1}^{N/2}\sum_{m=-N/2+1}^{N/2} \mathrm{i}(k_n + k_m)^\circ \widehat{f}_n \widehat{g}_m e^{\mathrm{i}(k_n+k_m)^\circ x_j}. \tag{2.7}$$

For modes that contribute to the aliasing error the Fourier coefficients are multiplied by the wavenumber of the resolved mode rather than the actual wavenumber.

It will be shown that the skew-symmetric form of the nonlinear term gives a reduced amplitude of the above aliasing error. Consider rewriting the derivative of the product as

$$\alpha \frac{\partial}{\partial x}(fg) + (1-\alpha)\left(\frac{\partial f}{\partial x} g + f \frac{\partial g}{\partial x}\right). \tag{2.8}$$

Upon substituting the Fourier representation for $f(x)$ and $g(x)$ and discretizing, this becomes

$$\sum_{n=-N/2+1}^{N/2} \sum_{m=-N/2+1}^{N/2} \mathrm{i}\left[\alpha(k_n + k_m)^\circ + (1-\alpha)(k_n + k_m)\right] \hat{f}_n \hat{g}_m \mathrm{e}^{\mathrm{i}(k_n + k_m)^\circ x_j}. \tag{2.9}$$

where the fact that $k^\circ = k$ for the resolved wavenumbers has been used. Since, for modes that create aliasing errors, $(k_n + k_m)^\circ \neq (k_n + k_m)$, the value of the derivative depends on the parameter α. When evaluated analytically, (2.8) is of course equivalent to (2.1) and independent of α. However, the product rule for differentiation used to obtain this form does not hold numerically.

Let $k^* = \left[\alpha(k_n + k_m)^\circ + (1-\alpha)(k_n + k_m)\right]$ be an effective wavenumber that multiplies the Fourier coefficients when a derivative is taken. For Fourier modes with $(k_n + k_m)$ within the range of resolved wavenumbers, there is no aliasing error, whereas for modes that create aliasing errors, k^* will affect the magnitude of the aliasing errors. Therefore, it may be possible to set the parameter α to reduce the aliasing error.

With $\alpha = 1$ we recover the original conservative form of the nonlinear term, while with $\alpha = 1/2$ we have the skew-symmetric form, and with $\alpha = 0$ we have the nonconservative form. A plot of k^* as a function of $(k_n + k_m)$ for the three values of α is shown in Fig. 2. (Only the range of $(k_n + k_m)$ that gives rise to aliasing errors is considered.) As seen in Fig. 2, the skew-symmetric form gives values of k^* that are small for modes with $(k_n + k_m)$ close to the range of resolved wavenumbers. Modes in this range come from a product of modes with intermediate wavenumbers or the product of a mode with a low wavenumber and a mode with a high wavenumber. The value of k^* for the skew-symmetric form is larger for higher values of $(k_n + k_m)$, and these modes come from products of two high wavenumber modes. For problems of physical interest, the solutions have Fourier coefficients that decay at high wavenumbers, and aliasing errors coming from the modes close to the resolved wavenumber range generally have higher amplitude than aliasing errors coming from higher wavenumber modes. Therefore, it is more important to suppress the aliasing errors coming from the region close to the resolved wavenumber range. Since the skew-symmetric form has a smaller amplitude for the aliasing errors coming from these modes than the other formulations, it is expected to perform better.

To determine if the reduction in aliasing errors is realized in practice we consider two problems. The first is the one-dimensional viscous Burgers' equation, and the second is a large-eddy simulation of compressible isotropic turbulence.

Although here we are considering the convective term, other nonlinear terms, such as diffusion terms with nonuniform transport coefficients, can be written in the skew-symmetric form. We believe aliasing errors would be reduced for these terms as well.

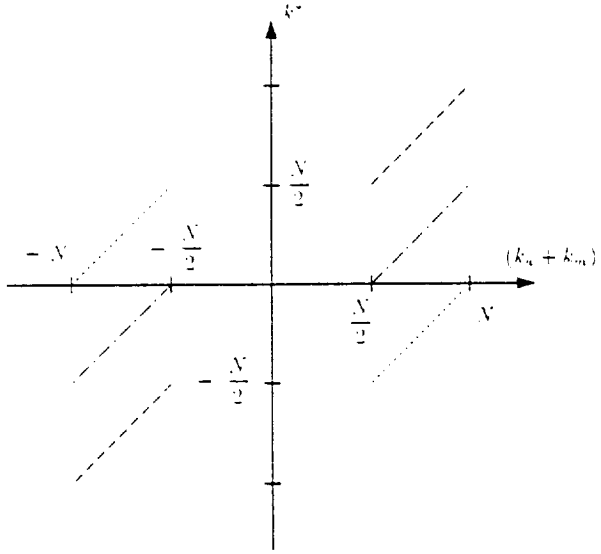

Fig. 2. Effective wavenumber in the derivative of a product. Conservative form, ·····, skew-symmetric form, – · –, nonconservative form, – – – –.

3. Burgers' equation model problem

As a model problem we consider the one-dimensional viscous Burgers' equation,

$$u_t + uu_x = \nu u_{xx}, \tag{3.1}$$

where a subscript denotes partial differentiation. Benton and Platzman [3] give several exact solutions and we choose their case (5.2) in which the boundary conditions are periodic and the initial conditions are given by $u(x,0) = -R\sin(x)$.

Burgers' equation was solved numerically using a Fourier pseudospectral method with a 5th order accurate Runge–Kutta–Fehlberg time advancement scheme [9]. The nonlinear convective term was formulated using the following three forms

$$\frac{1}{2}(u^2)_x, \tag{3.2}$$

$$\frac{1}{4}(u^2)_x + \frac{1}{2}uu_x, \tag{3.3}$$

$$uu_x, \tag{3.4}$$

which are the conservative, skew-symmetric and nonconservative forms respectively. The specific case we examine has $R = -20$ and was integrated to $t = 0.075$. The time step was $\Delta t = 0.0001$ and the time differencing errors were checked to ensure that they were negligible compared to the spatial differencing errors. The calculations were done on a Cray YMP for which the word length is 64 bits in an effort to keep round off error low.

The numerical solutions for $N = 32$ are compared to the exact solution in Fig. 3, and the maximum and r.m.s. errors are given in Table 1. At first the results are somewhat surprising because, while the

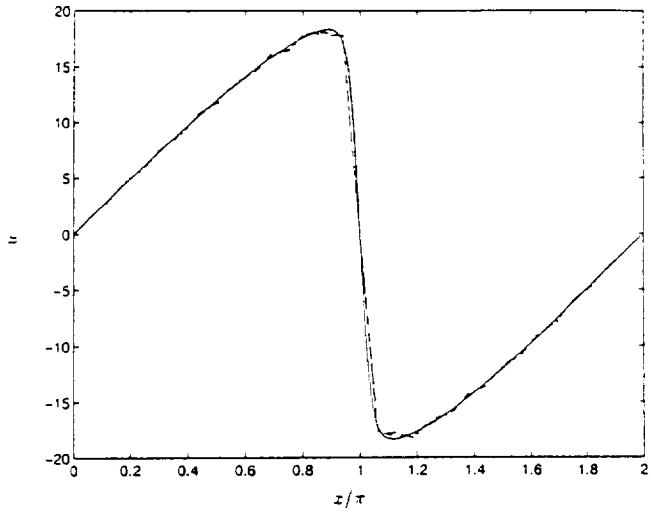

Fig. 3. Solution to Burgers' equation at $t = 0.075$ ($N = 32$). Exact solution. —, conservative form. · · · · · ·, skew-symmetric form. – · –, nonconservative form. – – – –.

Table 1
Maximum and r.m.s. errors in the numerical solution to Burgers' equation

		$N = 32$		$N = 33$	
Formulation	α	max	r.m.s.	max	r.m.s.
Conservative	1	1.11	0.127	1.10	0.056
Skew-symmetric	1/2	0.59	0.056	0.33	0.018
Nonconservative	0	0.46	0.026	3.14	0.202

skew-symmetric form performs better than the conservative form, it does worse than the nonconservative form. However, we found that if the calculations are done using $N = 33$ grid points, the results (given in Table 1) show the skew-symmetric form performs the best and the nonconservative form does the worst, by a large margin. This behavior seems perplexing; however, a detailed investigation gives some insight into the differences in the formulations.

The convective term was examined in detail to see the differences in the formulations. The exact solution $u(x, t)$ was calculated at $t = 0.075$ at the N collocation points, and then the convective term was formed using the three formulations. The magnitudes of the Fourier coefficients are shown in Figs. 4 and 5 for $N = 32$ and $N = 33$ respectively. Also shown are the Fourier coefficients for the exact convective term (the Fourier coefficients were obtained by transforming the exact convective term on $N = 256$ collocation points) and a dealiased convective term, which is described below. From Fig. 4 one finds that for $N = 32$ the Fourier coefficients from the nonconservative formulation lie the closest to those from the exact solution, while for $N = 33$ the Fourier coefficients from the skew-symmetric form are the closest. (Because of the symmetry of the problem, the phase of the Fourier coefficients is $\pm\pi/2$, and all of the numerical solutions have the same phase of the Fourier

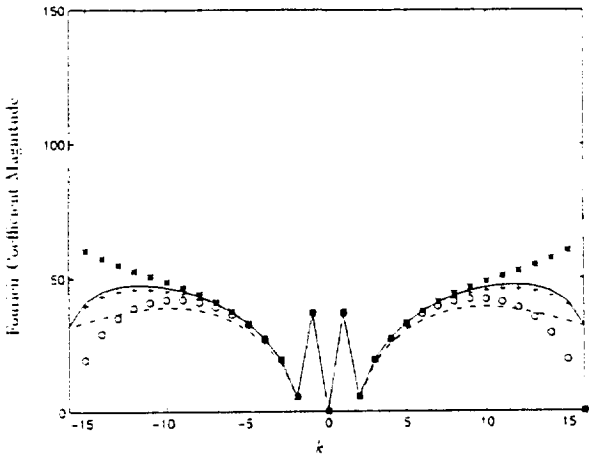

Fig. 4. Magnitude of the Fourier coefficients of the convective term formed using the exact solution at $t = 0.075$ on $N = 32$ grid points. Conservative form, *, skew-symmetric form, +, nonconservative form, ○, dealiased, —, exact, – – – –.

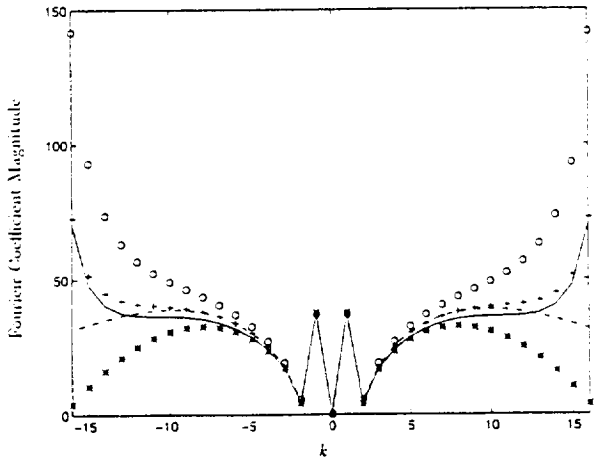

Fig. 5. Magnitude of the Fourier coefficients of the convective term formed using the exact solution at $t = 0.075$ on $N = 33$ grid points. Conservative form, *, skew-symmetric form, +, nonconservative form, ○, dealiased, —, exact, – – – –.

coefficients as the exact solution. Therefore, examination of the magnitude of the Fourier coefficients of the convective term gives a proper comparison.)

For $N = 32$ the magnitude of the Fourier coefficients for the conservative formulation are larger than those of the skew-symmetric form and those for the nonconservative formulation are smaller, while for $N = 33$ these relative positions are switched. The switching of the relative magnitude of the Fourier coefficients in the numerical solutions for $N = 32$ and $N = 33$ is due to the phase relationships among the Fourier coefficients of the solution. To see this, consider the factor $ik^* \widehat{f}_n \widehat{g}_m$ in (2.9). The phase of the Fourier coefficients of the exact solution are $\pi/2$ for even positive or odd negative mode

numbers, and $-\pi/2$ for odd positive or even negative mode numbers. So $\widehat{f}_n = \mathrm{i}\,\mathrm{sgn}(n)(-1)^n|\widehat{f}_n|$. For the modes that create aliasing errors, the factor can be written

$$\mathrm{i}\big[\alpha(k_n + k_m)^\diamond + (1-\alpha)(k_n + k_m)\big]\big[\mathrm{i}\,\mathrm{sgn}(n)(-1)^n|\widehat{f}_n|\big]\big[\mathrm{i}\,\mathrm{sgn}(m)(-1)^m|\widehat{g}_m|\big]$$
$$= \mathrm{i}\big[\alpha(k_n + k_m)^\diamond + (1-\alpha)(k_n + k_m)\big]|\widehat{f}_n||\widehat{g}_m|(-1)^{n+m+1}. \tag{3.5}$$

(Since the sign of n and m will be the same for modes contributing to the aliasing error, $\mathrm{sgn}(n)\mathrm{sgn}(m) = 1$.) If the product of modes n and m are aliased to mode l, then $l = n + m + \mathrm{sgn}(l)N$. The Fourier coefficients of the exact convective term have phases that are $\pm\pi/2$ with the sign opposite that of the coefficients for the solution (with the exception of the $l = \pm 1$ modes). Pulling out a factor to account for the phase we have

$$\big[\mathrm{i}\,\mathrm{sgn}(l)(-1)^{(l+1)}\big]\mathrm{sgn}(l)\big[\alpha(k_n + k_m)^\diamond + (1-\alpha)(k_n + k_m)\big]|\widehat{f}_n||\widehat{g}_m|(-1)^{-\mathrm{sgn}(l)N}. \tag{3.6}$$

Therefore, the aliasing error will be multiplied by (± 1) depending on whether the number of collocation points, N, is even or odd. The error is either added or subtracted depending on the the parity of N and the sign of k^*, which is opposite for $\alpha = 0$ and $\alpha = 1$.

As an example, consider $l = 15$. With $N = 32$ the Fourier modes that contribute to the aliasing error are $(n, m) = \{(-15, -2), (-14, -3), \ldots, (-2, -15)\}$. The factor in equation (3.6), without the phase term, is

$$\big[\alpha(15) + (1-\alpha)(-17)\big]|\widehat{f}_n||\widehat{g}_m|(-1)^{-32} = \big[32\alpha - 17\big]|\widehat{f}_n||\widehat{g}_m|. \tag{3.7}$$

For $\alpha = 1,\ 1/2,\ 0$ the factor in the brackets is 15, -1 and -17, which corresponds very well to the relative magnitudes of the differences between the Fourier coefficients of the numerical solutions and the dealiased result for mode 15 in Fig. 4. With $N = 33$ the Fourier modes that contribute to the aliasing error are $(n, m) = \{(-16, -2), (-15, -3), \ldots, (-2, -16)\}$. The factor in equation (3.6), without the phase term, is

$$\big[\alpha(15) + (1-\alpha)(-18)\big]|\widehat{f}_n||\widehat{g}_m|(-1)^{-33} = \big[18 - 33\alpha\big]|\widehat{f}_n||\widehat{g}_m|. \tag{3.8}$$

For $\alpha = 1,\ 1/2,\ 0$ the factor in the brackets is -15, 1.5 and 18, which again correspond very well to the results for mode 15 in Fig. 5. Therefore, we can understand the large shift in the error in the convective term observed when N is changed.

To see the aliasing errors produced by the three formulations they are compared to a dealiased result in which the aliasing errors have been eliminated. Forming the product uu_x creates Fourier modes with mode numbers $-N, \ldots, N$, which would require $2N$ collocation points to represent. A dealiased convective term is formed by starting with u on N collocation points, transforming to wave space, padding the Fourier coefficients with zeros so that at least $2N$ Fourier coefficients are used (we used 256 modes, although this is unnecessary), forming the Fourier transform of u_x, transforming u and u_x back to physical space on the larger number of collocation points, forming the product, transforming to wave space, and keeping only the N Fourier coefficients. This is the method that was used to compute the curve labeled "dealiased convective term" in Figs. 4 and 5. One sees that the skew-symmetric form is very close to the dealiased form, as one would expect from the analysis in Section 2. Therefore, the skew-symmetric form of the convective term gives a viable alternative to dealiasing. Note that dealiasing is very expensive for the compressible Navier–Stokes equations because of the extra Fourier transforms needed. Although dealiasing is used for incompressible turbulence simulations, it is not practical for the compressible equations.

However, as is clear in Figs. 4 and 5, the dealiased convective term is not the same as the exact convective term. This is because the exact solution cannot be represented by a finite number of Fourier modes, and so the Fourier coefficients computed using $N = 32$ or $N = 33$ collocation points are not the exact Fourier coefficients. The difference is due to truncation error. Just as with the aliasing errors, the value of the truncation error is determined by the phase relationships of the exact Fourier coefficients of the solution. Because of the symmetry of the solution, the parity of N can make a large difference in the truncation error, as is clear in the difference between the dealiased solutions in Figs. 4 and 5. With this understanding one can see that the low value of the error in the convective term for the nonconservative formulation with $N = 32$ is due to aliasing errors partially canceling truncation errors, whereas with $N = 33$ aliasing errors add with the truncation errors to produce a very large error.

From the above analysis we see that the low error for the nonconservative formulation on $N = 32$ grid points is fortuitous and is due to the particular symmetry properties of the solution. Although the skew-symmetric form of the convective term does not give the least error in all cases, it is the most robust. For problems, such as the simulation of turbulence, where the solution has a more random distribution of phases of the Fourier coefficients than for the solution of Burgers' equation, the skew-symmetric form is expected to perform better than the other formulations. In the next section we examine the behavior of the various formulations applied to large-eddy simulation of turbulence. The above example also points out the danger of drawing conclusions about numerical methods based on simple problems, although such problems are useful in understanding how a numerical method works.

4. Large-eddy simulation

The problem we are interested in is the simulation of turbulent flows, specifically compressible homogeneous turbulence. One approach is direct numerical simulation (DNS), in which the time dependent Navier–Stokes equations are solved without any kind of turbulence model. However, because of the wide range of length scales that occur in turbulence, DNS is limited by current computer capability to low Reynolds numbers. A means of simulating flows at higher Reynolds numbers is to perform large-eddy simulations (LES), in which the motion of the large eddies are resolved, while the effects of eddies smaller than the grid spacing are modeled. Aliasing errors occur in both DNS and LES; however, since large-eddy simulations are by definition not well resolved, aliasing errors are a more important issue with LES than with DNS.

The large-eddy simulations used are discussed in detail in [15], so only a brief overview will be given here. The simulations are of decaying isotropic compressible turbulence. The computer program uses a Fourier pseudospectral collocation method with a compact storage third order Runge–Kutta time advancement scheme. The computations were performed on a Cray C90.

The convective terms in the momentum and internal energy equation were written in the general form

$$\alpha \frac{\partial}{\partial x_j}(f_i g_j) + (1-\alpha)\left(f_i \frac{\partial g_j}{\partial x_j} + \frac{\partial f_i}{\partial x_j} g_j\right), \tag{4.1}$$

where in the momentum equation $f_i = \rho u_i$ and $g_j = u_j$, while in the energy equation $f_i = \rho C_v T$ and $g_j = u_j$. (Note that the internal energy equation is solved in LES of compressible turbulence,

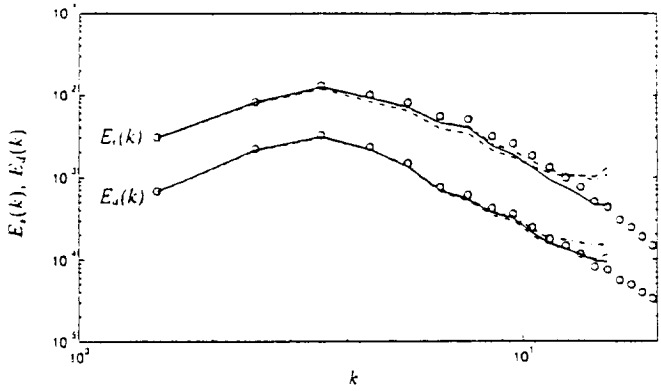

Fig. 6. Decomposed velocity spectra from LES of compressible isotropic turbulence. Solenoidal spectra, $E_s(k)$, dilatational spectra, $E_d(k)$. Conservative form, – – – –, skew-symmetric form, —, nonconservative form, – · –, DNS data, ○.

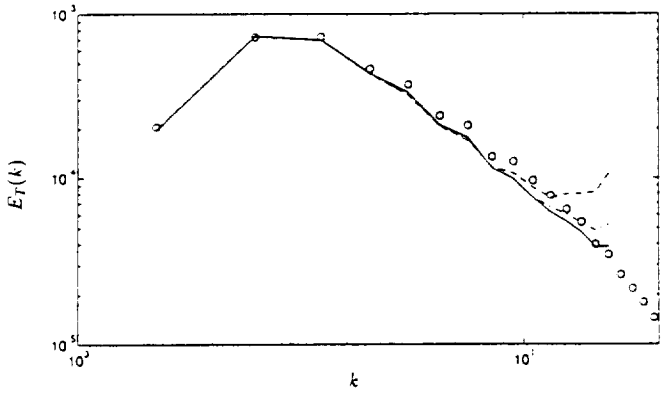

Fig. 7. Temperature spectra from LES of compressible isotropic turbulence. Conservative form, – – – –, skew-symmetric form, —, nonconservative form, – · –, DNS data, ○.

rather than the total energy equation, because of the difficulty in modeling additional terms that arise with the use of the total energy. See [7] and [15] for a discussion.) Setting $\alpha = 1$, $1/2$ or 0 gives the conservative, skew-symmetric, and nonconservative formulations respectively.

The conditions used are those of case (6) in [15] for which the initial turbulent Mach number is 0.4, and the grid has 32^3 points. In order to see the differences in the effect of the formulations, we examined the three-dimensional power spectral density of the velocity field, decomposed into solenoidal and dilatational parts, and the temperature field, $E_s(k)$, $E_d(k)$ and $E_T(k)$ respectively. The velocity spectra are shown in Fig. 6 and the temperature spectra are shown in Fig. 7, at a time when the turbulence has decayed for two initial eddy turnover times. Also shown for comparison are the results from a DNS using 128^3 grid points. The results for the conservative formulation and the nonconservative formulation show an unphysical pile-up in the spectra at high wavenumber k. This behavior is due to aliasing errors. The skew-symmetric formulation results, on the other hand, show very little pile-up

in the spectrum. As an additional test, simulations were also done on a higher Reynolds number case, which corresponds to the experiment of Compte-Bellot and Corrsin [6]. The conservative form and the nonconservative form resulted in numerical instabilities that halted the simulations, while the skew-symmetric form resulted in a simulation that was completed and compared well with the experimental data. These results show that the skew-symmetric formulation of the convective terms reduces aliasing errors and produces a more accurate solution than the conservative and nonconservative formulations.

5. Conclusion

The effect of the formulation of the nonlinear convective term on aliasing errors has been examined. A Fourier analysis using an effective wavenumber shows that the skew-symmetric form of the convective term results in a reduced amplitude of the aliasing errors compared to the conservative and nonconservative forms. The three formulations of the convective term were tested for Burgers' equation. It was found that in some cases the nonconservative form gives the lowest total error rather than the skew-symmetric form. However, a detailed Fourier analysis of the convective term shows that the behavior of the formulations is dependent on the phase relationships of the Fourier coefficients of the solution, and that the skew-symmetric form gives the most robust results of the three. The three formulations were tested in the large-eddy simulation of decaying compressible isotropic turbulence, and it was found that the skew-symmetric form gives the most accurate results, consistent with the error analysis.

Acknowledgements

This work was supported in part by the NASA Langley Research Center under grant NAG 1–1509. Computer resources were provided by NAS, NCSA and Purdue University.

References

[1] J.R. Anderson, A local, minimum aliasing method for use in nonlinear numerical models, *Monthly Weather Review* 117 (1989) 1369–1379.

[2] A. Arakawa, Computational design for long-term numerical integration of the equations of fluid motion: two-dimensional incompressible flow, Part I, *J. Comput. Phys.* 1 (1966) 119–143.

[3] E.R. Benton and G.W. Platzman, A table of solutions of the one-dimensional Burgers' equation, *Quart. Appl. Math.* 30 (1972) 195–212.

[4] G.A. Blaisdell, N.N. Mansour and W.C. Reynolds, Numerical simulations of compressible homogeneous turbulence, Report TF–50, Department of Mechanical Engineering, Stanford University, Stanford, CA (1991).

[5] C. Canuto, M.Y. Hussaini, A. Quarteroni and T.A. Zang, *Spectral Methods in Fluid Dynamics* (Springer, Berlin, 1988).

[6] G. Compte-Bellot and S. Corrsin, Simple Eulerian time correlation of full and narrow band velocity signals in grid generated isotropic turbulence, *J. Fluid Mech.* 48 (1971) 273–337.

[7] G. Erlebacher, M.Y. Hussaini, C.G. Speziale and T.A. Zang, Toward the large-eddy simulation of compressible turbulent flows, *J. Fluid Mech.* 238 (1992) 155–185.

[8] W.J. Feiereisen, W.C. Reynolds and J.H. Ferziger, Numerical simulation of a compressible, homogeneous, turbulent shear flow, Report TF–13, Department of Mechanical Engineering, Stanford University, Stanford, CA (1981).

[9] J.D. Hoffman, *Numerical Methods for Engineers and Scientists* (McGraw-Hill, New York, 1992).

[10] K. Horiuti, Comparison of conservative and rotational forms in large eddy simulation of turbulent channel flow, *J. Comput. Phys.* 71 (1987) 343–370.

[11] D. Kwak, Three-dimensional time dependent computation of turbulent flow, Ph.D. Thesis, Department of Mechanical Engineering, Stanford University, Stanford, CA (1975).

[12] N.N. Mansour, P. Moin, W.C. Reynolds and J.H. Ferziger, Improved methods for large eddy simulation of turbulence, in: F. Durst, B.E. Launder, F.W. Schmidt and J.H. Whitelaw, eds., *Turbulent Shear Flows I* (Springer, Berlin, 1979) 386–401.

[13] S.A. Orszag, On the elimination of aliasing in finite-diferencing schemes by filtering high-wavenumber components, *J. Atmospheric Sci.* 28 (1971) 1074.

[14] N.A. Philips, An example of nonlinear computational instability, in: *The Atmosphere and the Sea in Motion* (Rockefeller Institute Press and the Oxford University Press, New York, 1959) 501–504.

[15] E.T. Spyropoulos and G.A. Blaisdell, Evaluation of the dynamic subgrid-scale model for large eddy simulations of compressible turbulent flows, AIAA Paper 95–0355, 33rd Aerospace Sciences Meeting, AIAA, 1995.

[16] T.A. Zang, On the rotational and skew-symmetric forms for incompressible flow simulations, *Appl. Numer. Math.* 7 (1991) 27–40.

Attachment C

Extended Abstract submitted to the
35th AIAA Aerospace Sciences Meeting and Exhibit
Reno, NV, January 6–9, 1997

Large-Eddy Simulation of a Spatially Evolving Compressible Boundary Layer Flow

Evangelos T. Spyropoulos and Gregory A. Blaisdell
School of Aeronautics and Astronautics
Purdue University
W. Lafayette, Indiana

May 1996

Introduction

In the past few years, there has been a resurgence of interest in performing large-eddy simulations (LES) of flows of engineering interest. There are two roles for LES to play in the computation of complex turbulent flows. First, LES can be used to study the physics of turbulence at higher Reynolds numbers than can currently be achieved with direct numerical simulation (DNS) and LES can aid in the testing and improvement of lower order engineering turbulence models. Second, it is hoped that LES can be used in the near future as an engineering tool rather than as a research tool. Although it will remain an expensive tool, it might be the only means of accurately computing complex flows for which lower order models fail.

The majority of LES reported in the literature involve incompressible fluid flows that are homogeneous in at least two spatial directions. While computation of such flows has greatly contributed to the development of LES, the computation of more complex flows is required. In this paper, the method is applied to a spatially-developing compressible boundary layer flow. Several issues related to the effect of the numerical scheme on the simulations are investigated. A high-order, upwind biased, implicit, finite difference scheme is employed in the simulations and subgrid-scale (SGS) modeling is performed using the dynamic model.

Mathematical Formulation

In large-eddy simulation (LES) one computes explicitly only the motion of the large-scale structures. The nonlinear interactions with the small-scales are not resolved by the numerical grid and are modeled. The governing equations for the large eddies in compressible flows are obtained after filtering the continuity, momentum, and energy equations and recasting in terms of Favre averages. The filtering operation (denoted by an overbar) maintains only the large-scales and can be written in terms of a convolution integral,

$$\overline{f}(x_1, x_2, x_3) = \int_D \prod_{i=1}^{3} G_i(x_i - x_i') f(x_1', x_2', x_3') dx_1' dx_2' dx_3' \,. \tag{1}$$

where f is a turbulent field, G_i is some spatial filter that operates in the i-th direction and has a filter width, Δ_i (usually equal to the computational grid spacing in that direction) and D is the flow domain.

The resulting equations of motion for the large eddies are as follows:

$$\frac{\partial \overline{\rho}}{\partial t} + \frac{\partial (\overline{\rho}\tilde{u}_i)}{\partial x_i} = 0 \,, \tag{2}$$

$$\frac{\partial (\overline{\rho}\tilde{u}_i)}{\partial t} + \frac{\partial (\overline{\rho}\tilde{u}_i\tilde{u}_j)}{\partial x_j} = -\frac{\partial \overline{p}}{\partial x_i} + \frac{\partial}{\partial x_j}\left[\tilde{\mu}\left(\frac{\partial \tilde{u}_i}{\partial x_j} + \frac{\partial \tilde{u}_j}{\partial x_i} - \frac{2}{3}\frac{\partial \tilde{u}_k}{\partial x_k}\delta_{ij}\right) - \tau_{ij}\right] \,, \tag{3}$$

$$\frac{\partial \overline{p}}{\partial t} + \frac{\partial (\overline{p}\tilde{u}_i)}{\partial x_i} = (\gamma - 1)\left\{-\overline{p}\frac{\partial \tilde{u}_i}{\partial x_i} + \tilde{\mu}\left(\frac{\partial \tilde{u}_i}{\partial x_j} + \frac{\partial \tilde{u}_j}{\partial x_i} - \frac{2}{3}\frac{\partial \tilde{u}_k}{\partial x_k}\delta_{ij}\right)\frac{\partial \tilde{u}_j}{\partial x_i} + \frac{\partial}{\partial x_i}\left(\tilde{k}\frac{\partial \tilde{T}}{\partial x_i} - q_i\right)\right\} \,. \tag{4}$$

The effects of the small-scales are present in the above equations through the SGS stress tensor and the SGS heat flux,

$$\tau_{ij} = \overline{\rho}\left(\widetilde{u_i u_j} - \tilde{u}_i\tilde{u}_j\right) \,, \tag{5}$$

$$q_i = \overline{\rho}\left(\widetilde{u_i T} - \tilde{u}_i\tilde{T}\right) \,, \tag{6}$$

respectively, and require modeling. A tilde is used to denote Favre averages ($\tilde{f} = \overline{\rho f}/\overline{\rho}$). Also, ρ is the density, T is the temperature, u_i is the velocity component in the i-direction and k is the thermal conductivity. The specific heats at constant volume, C_v, and at constant pressure, C_p, are assumed in this study to be constant. The large-scale molecular viscosity, $\tilde{\mu}$, is assumed to obey Sutherland's law,

$$\frac{\tilde{\mu}}{\tilde{\mu}_0} = \left(\frac{\tilde{T}}{\tilde{T}_0}\right)^{3/2}\frac{\tilde{T}_0 + \tilde{T}_e}{\tilde{T} + \tilde{T}_e} \,, \tag{7}$$

with a Sutherland constant $\tilde{T}_e = 198.6^\circ R$. The large-scale pressure, $\overline{p}$, is obtained from the filtered equation of state,

$$\overline{p} = \overline{\rho}R\tilde{T} \,. \tag{8}$$

The molecular Prandtl number, Pr, is assumed to be 0.718. Note, that in deriving Eqs. (2)-(4), the viscous, pressure-dilatation and conduction terms were approximated in a similar fashion as by Erlebacher *et al.*[1] For example, the pressure dilatation term is approximated as follows:

$$\overline{p\frac{\partial u_i}{\partial x_i}} = \overline{\rho RT\frac{\partial u_i}{\partial x_i}} = \overline{\rho}R\widetilde{T\frac{\partial u_i}{\partial x_i}} = \overline{\rho}R\tilde{T}\frac{\partial \tilde{u}_i}{\partial x_i} + \overline{\rho}R\left(\widetilde{T\frac{\partial u_i}{\partial x_i}} - \tilde{T}\frac{\partial \tilde{u}_i}{\partial x_i}\right) \simeq \overline{p}\frac{\partial \tilde{u}_i}{\partial x_i} \,. \tag{9}$$

In the above, the small-scale temperature dilatation terms in the parentheses are neglected, since they are expected to have a small influence on the large-scales compared to the SGS heat flux, q_i, and also because they are very difficult to model.[2,1,3]

Subgrid-Scale Modeling

The dynamic SGS modeling concept was introduced by Germano *et al.*[4] for LES of incompressible flows and has attracted a lot of attention in the LES community during the

recent years. Moin *et al.*[3] extented the dynamic model to compressible flows and Lilly[5] suggested a refinement to both models that is now largely employed. Since then, further refinements to the model have been proposed (Wong,[6] Ghosal *et al.*,[7] Piomelli *et al.*[8]).

The model for the deviatoric and isotropic parts of the SGS stress tensor is based on Smagorinski's[9] and Yoshizawa's[10] eddy-viscosity models, respectively. The model constants, however, are allowed to vary in space and time, and are computed dynamically, as the simulation progresses, from the energy content of the smallest of the resolved large-scales. This approach of calculating the model constants has been found to substantially improve the accuracy and robustness of the LES method, since the model constants adjust dynamically to the local structure of the flow and do not have to be specified *a priori*. In addition, it has been found from incompressible flow simulations, that the dynamic model provides the correct limiting behavior near solid boundaries, and adjusts properly by itself in the transitional or laminar regimes. Although it can not predict properly backscatter, it allows for some reverse energy cascade. A similar approach is followed for the SGS heat flux.

Dynamic modeling is accomplished with the aid of a second filter (referred to as the *test filter*, $\widehat{G}$) that has a filter width $\widehat{\Delta}_i$ in the i-th direction, that is coarser than the grid used to perform the computations ($\widehat{\Delta}_i > \Delta_i$).

The model parameterization for the SGS stress and the SGS heat flux is given by

$$\tau_{ij} - \frac{1}{3}\tau_{kk}\delta_{ij} = -2\mu_t\left(\tilde{S}_{ij} - \frac{1}{3}\tilde{S}_{kk}\delta_{ij}\right) , \tag{10}$$

$$\tau_{kk} = 2C_I\overline{\rho}\Delta^2|\tilde{S}|^2 , \tag{11}$$

$$q_i = -k_t\frac{\partial\tilde{T}}{\partial x_i} . \tag{12}$$

where $\mu_t = C\Delta^2\overline{\rho}|\tilde{S}|$, $k_t = \mu_t/Pr_t$, $\tilde{S}_{ij} = 0.5\left(\partial\tilde{u}_i/\partial x_j + \partial\tilde{u}_j/\partial x_i\right)$, $|\tilde{S}| = \left(2\tilde{S}_{ij}\tilde{S}_{ij}\right)^{1/2}$, and $\Delta = (\Delta x\Delta y\Delta z)^{1/3}$.

The model coefficients are computed from

$$C = \frac{\langle\left(\mathcal{L}_{ij} - \frac{1}{3}\mathcal{L}_{kk}\delta_{ij}\right)M_{ij}\rangle}{\langle M_{pq}M_{pq}\rangle} , \tag{13}$$

$$C_I = \frac{\langle\mathcal{L}_{kk}\rangle}{\left\langle 2\widehat{\Delta}^2\widehat{\overline{\rho}}|\widehat{\tilde{S}}|^2 - 2\Delta^2\widehat{\overline{\rho}|\tilde{S}|^2}\right\rangle} . \tag{14}$$

$$Pr_t = C\frac{\langle N_iN_i\rangle}{\langle -K_jN_j\rangle} , \tag{15}$$

where $\widehat{\ }$ denotes test-filtered quantities, $\widehat{\Delta} = \left(\widehat{\Delta}_1\widehat{\Delta}_2\widehat{\Delta}_3\right)^{1/3}$ ($\widehat{\Delta}_i$ is the width of the test filter in the ith direction), $\langle\ \rangle$ denotes averaging over the homogeneous spanwise direction, and

$$\mathcal{L}_{ij} = \widehat{\overline{\rho}\tilde{u}_i\tilde{u}_j} - \frac{1}{\widehat{\overline{\rho}}}\widehat{\overline{\rho}\tilde{u}_i}\,\widehat{\overline{\rho}\tilde{u}_j} . \tag{16}$$

$$M_{ij} = -2\hat{\Delta}^2\hat{\overline{\rho}}|\hat{\tilde{S}}|\left(\hat{\tilde{S}}_{ij} - \frac{1}{3}\hat{\tilde{S}}_{kk}\delta_{ij}\right) + 2\widehat{\Delta^2\overline{\rho}|\tilde{S}|\left(\tilde{S}_{ij} - \frac{1}{3}\tilde{S}_{kk}\delta_{ij}\right)}\,. \tag{17}$$

$$N_i = \hat{\Delta}^2\hat{\overline{\rho}}|\hat{\tilde{S}}|\frac{\partial\hat{\tilde{T}}}{\partial x_i} - \widehat{\Delta^2\overline{\rho}|\tilde{S}|\frac{\partial\tilde{T}}{\partial x_i}}\,, \tag{18}$$

$$K_i = \widehat{\overline{\rho}\tilde{u}_i\tilde{T}} - \frac{1}{\hat{\overline{\rho}}}\widehat{\overline{\rho}\tilde{u}_i}\,\widehat{\overline{\rho}\tilde{T}}\,, \tag{19}$$

In the simulations, negative values for the eddy viscosity, μ_t, and eddy conductivity, k_t, were allowed, as long as the total viscosity ($\mu_T = \tilde{\mu} + \mu_t$) and the total thermal conductivity ($k_T = \tilde{k} + k_t$) were non-negative. In terms, this restricts the amount of energy back-scatter allowed, but avoids numerical instabilities due to anti-dissipation. A three-point top-hat filter (derived using the trapezoidal integration rule) was employed for the test filtering.

Numerical Method

The DNS code of Rai *et al.*[11] was modified to perform LES using the dynamic model. The DNS code solves the Navier-Stokes equations in non-conservative form. Since the problem considered here does not exhibit discontinuities, the same approach was taken in the LES to solve Eqs. (2)-(4). Spatial derivatives are computed using fifth-order-accurate upwind-biased differences for the convective terms and fourth-order-accurate central differences for the viscous terms. Fourth-order-accurate central differences are also used to compute the spatial derivatives in the dynamic model. Time advancement is performed using an iterative fully implicit second-order-accurate scheme.[12] Such schemes are unconditionally stable and allow for accurate advancement using much larger time steps than explicit schemes. However, they are more CPU intensive, since they involve the solution of a system of algebraic equations. In addition, upwind schemes are much more stable than central difference schemes, since they provide implicitly some artificial dissipation (this controls also aliasing errors).

Reference Case and Calculation Set-up

The experimental configuration of Shutts *et al.*[13] was chosen as a test case. It is that of a zero-pressure gradient, flat-plate boundary layer flow at $M = 2.25$. The Reynolds number based on inlet conditions is 635000/in. The adiabatic wall temperature is $580^o R$ and the temperature at the freestream is $305^o R$.

The size of the computational domain and the type of boundary conditions are chosen the same as in the DNS.[11] for consistency. The computational domain is divided along the streamwise direction in three regions. The first region is 2.5in. long and contains the regions of blowing and suction, as well as transition. The second region has uniform spacing in x, is 2in. long, and contains the turbulent region. The third region is 6in. long and gradually becomes very coarse to artificially damp the turbulent fluctuations and ensure that the outlet boundary will be non-reflective. The domain is 0.35in. wide in the span, and 3in. tall along the wall-normal direction.

Periodic blowing and suction is imposed on the flat plate, at a distance of 0.5in. from the inlet, to trip the incoming flow to turbulence. The wall-normal velocity at the plate in this region is as follows:

$$v = Au_\infty f(x)g(z)h(t)\,. \tag{20}$$

where

$$f(x) = 4sin\theta(1 - cos\theta)/27^{1/2} \ , \quad \theta = 2\pi(x - x_a)/(x_b - x_a) \ ,$$

$$g(z) = \sum_{l=0}^{l_{max}} Z_l sin(2\pi l(z/z_{max} + \phi_l)) \ , \quad \sum_{l=0}^{l_{max}} Z_l = 1 \ , \ Z_l = 1.25 Z_{l+1} \ ,$$

$$h(t) = \sum_{m=0}^{m_{max}} T_m sin(2\pi m(\beta t + \phi_m)) \ , \quad \sum_{m=1}^{m_{max}} T_m = 1 \ , \quad T_m = 1.25 T_{m+1} \ .$$

and $l_{max} = 10$, $m_{max} = 5$, $x_a = 4.5$in., $x_b = 5$in., $\mathcal{A} = 0.04$ is the disturbance amplitude. $\beta = 75000$Hz, ϕ_l, ϕ_m are random numbers (between 0 and 1), and $z_{max} = 0.35$in.

A no-slip boundary condition, together with an adiabatic wall temperature condition, is imposed on the rest of the flat plate. The conditions at the inflow and outflow boundaries are supersonic, except for the subsonic portion of the boundary layer. At the inflow boundary, the dependent variables are fixed based on results from a laminar boundary layer analysis. A non-reflecting boundary condition is specified at the outflow boundary, as was mentioned above. Periodic boundary conditions are used in the homogeneous spanwise direction. The computational domain is chosen such that it is long enough along the span to ensure that the flow is homogeneous in this direction. Finally, a symmetry boundary condition is imposed at the upper boundary, which is located well outside the boundary layer.

Preliminary Results

A number of simulations were conducted to examine several issues regarding the accuracy of the LES method in computing spatially evolving compressible boundary layer flows using finite difference schemes. The cases considered are summarized in Table 1.

Shown in figure 1 is the variation of the computed skin-friction coefficient, C_f, along the streamwise direction from simulations conducted at several different grid resolutions. The results are compared against the experimental data, the turbulent correlation of White and Christoff,[14] and the data from a marginally resolved DNS.[11] As the grid was refined the accuracy of the LES results improved. Case 2 uses 1/16 the number of grid points used in the DNS. This coarse grid simulation clearly under-predicts the skin friction, and appears to be at a much lower turbulence level close to the end of the well resolved region (x=8.8in.) When the grid was refined (case 3) the results improved. The number of grid points along the spanwise direction was finally doubled (case 4) to capture better the large-scale structures. That simulation employed 1/3 the number of grid points used in the DNS.

The variation of the Van Driest velocity (normalized by the shear stress at the wall) with the normal distance from the wall at x=8.8in. is shown in figure 2. Refining the grid again improved the agreement with the compressible law of the wall. Although the grid used in case 4 is only about a factor of 3 coarser than the DNS, there seems to still be room for improvement in accuracy.

The skin-friction distribution from simulations performed at higher disturbance levels (cases 5) is shown in figure 3. As expected, the location of transition is moved further upstream as the disturbance amplitude is gradually increased. However, no difference on C_f are observed at x=8.8in., indicating that the flow there is fully turbulent. Therefore, the differences seen in the LES in figures 1 and 2, are not due to any end stage (by-pass) transition phenomena.

The effect of the numerical method was examined by employing a lower order accurate scheme in the simulations. The convective terms were computed using third-order upwind differences. Second-order central differences were used in computing the diffusion terms and the derivatives in the dynamic model. A significant drop in the computed skin-friction coefficient was found when the lower order scheme was employed, as is shown for cases 7 and 8 in figure 4. This figure also shows that the lower order scheme required about 2.65 times more grid points to match the results of the higher-order scheme.

The final paper will contain comparisons of other boundary-layer statistics, such as profiles of turbulence intensities. In brief, they have been found to compare similarly to the above results.

Overall, the poor performance of the LES is believed to be mainly due to the truncation errors from the upwind scheme, rather than due to the dynamic SGS model. These errors artificially damp the turbulence of the smaller resolved scales. Subgrid scales contain less energy than the grid scales. As a result, even accurate modeling of subgrid scales will not overcome the errors due to the finite difference scheme. Furthermore, since the dynamic model predicts the eddy viscosity and eddy conductivity based on the turbulence level of the smallest resolved scales, it provides insufficient amounts of turbulent transport. Since the highly accurate spectral methods are not appropriate for use in complex flows, a possible solution to the problem would be to maintain only the information on the grid scales that are accurately resolved by a finite difference type scheme, while modeling the effects of the scales that are omited (including, of course, the subgrid scales). This approach, however, will substantially increase the cost of the simulation, since it would require explicit filtering of the contaminated modes at each time step using a high-order digital filter, and the use of finer grids to ensure that the remaining resolved scales adequately represent the large-eddies.

Conclusions

A number of issues involved in the LES of a spatially evolving compressible boundary layers are examined by conducting simulations using a high-order-accurate finite difference scheme and the dynamic SGS model. The computational grid was refined successively to improve the agreement of the computed turbulence statistics with the available experimental data and results from a marginally resolved DNS. The grids used in the LES were from 16 up to 3 times coarser than the grid used in the DNS. The computational domain was found to be long enough for the flow to reach a fully-turbulent state and free of transients due to the periodic blowing and suction mechanism employed to by-pass the natural transition process.

The results suggest that the finite difference scheme has a direct effect on the effectiveness of the SGS model influencing greatly the accuracy of the simulations. The use of higher-order scheme is found to improve substantially the results, since it improves the capture of the smaller resolved scales. Furthermore, it is recommended to apply the model not only at the subgrid-scales, but also at the scales that are not properly resolved by the numerical scheme.

Acknowledgements

This work was supported in part by NASA Langley Research Center under Grant No. NAG-1-1509.

References

[1] Erlebacher, G., Hussaini, M. Y., Speziale, C. G. and Zang, T. A., 1992. "Toward the large-eddy simulation of compressible turbulent flows," *J. Fluid Mech.* **238**, pp. 155–185.

[2] Sarkar, S., Erlebacher, G., Hussaini, M. Y. and Kreiss, H. O., 1991. "The analysis and modeling of dilatational terms in compressible turbulence," *J. Fluid Mech.* **227**, pp. 473–493.

[3] Moin, P., Squires, K., Cabot, W. and Lee, S., 1991. "A dynamic subgrid-scale model for compressible turbulence and scalar transport," *Phys. Fluids A.* **3**, pp. 2746–2757.

[4] Germano, M., Piomelli, U., Moin, P. and Cabot, W., 1991. "A dynamic subgrid-scale eddy-viscosity model," *Phys. Fluids A.* **3**, pp. 1760–1765.

[5] Lilly, D. K., 1992. "A proposed modification of the Germano subgrid-scale closure method," *Phys. Fluids A.* **4**, pp. 633–635.

[6] Wong, V. C., 1992. "A proposed statistical-dynamic closure method for the linear or nonlinear subgrid-scale stresses," *Phys. Fluids A.* **5**, pp. 1080–1082.

[7] Ghosal, S., Lund, T. S. and Moin, P., 1992. "A local dynamic model for large eddy simulation," *Center for Turbulence Research, Annual Research Briefs-1992, Stanford University, Stanford, California*, pp. 3–25.

[8] Piomelli, U. and Liu, J., 1994. "Large eddy simulation of rotating channel flows using a localized dynamic model," AGARD-CP-551; 74th AGARD/FDP Symposium on *Application of Direct and Large Eddy Simulation to Transition and Turbulence*, Chania, Greece.

[9] Smagorinski, J. S., 1963. "General circulation experiments with the primitive equations. I. The basic experiment," *Monthly Weather Review*, **91**, pp. 99–164.

[10] Yoshizawa, A., 1986. "Statistical theory for compressible turbulent shear flows, with the application to subgrid modeling," *Physics of Fluids A*, **29**(7), pp. 2152–2164.

[11] Rai, M. M., Gatski, T. B. and Erlebacher, G., 1995. "Direct simulation of spatially evolving compressible turbulent boundary layers," AIAA Paper 95-0583, 33rd AIAA Aerospace Sciences Meeting, Reno, NV.

[12] Rai, M. M. and Moin, P., 1993. "Direct numerical simulation of transition and turbulence in a spatially evolving boundary layer," *Journal of Computational Physics*, **109**, pp. 169–192.

[13] Fernholz, H. H. and Finley, P. J., 1977. "A critical compilation of compressible turbulent boundary layer data," *AGARDograph No. 223*, Case 55010501.

[14] White, F. M., 1991. *Viscous Fluid Flow*, McGraw-Hill Book Company.

Table 1: Case parameters

Case	Type	Grid Size	$\mathcal{A}$
1	DNS, 4th order	$971 \times 55 \times 321$	0.04
2	LES, 4th order	$311 \times 55 \times 65$	0.04
3	LES, 4th order	$416 \times 55 \times 129$	0.04
4	LES, 4th order	$416 \times 55 \times 257$	0.04
5	LES, 4th order	$311 \times 55 \times 65$	0.10
6	LES, 4th order	$416 \times 55 \times 129$	0.06
7	LES, 2nd order	$311 \times 55 \times 65$	0.04
8	LES, 2nd order	$416 \times 55 \times 129$	0.04

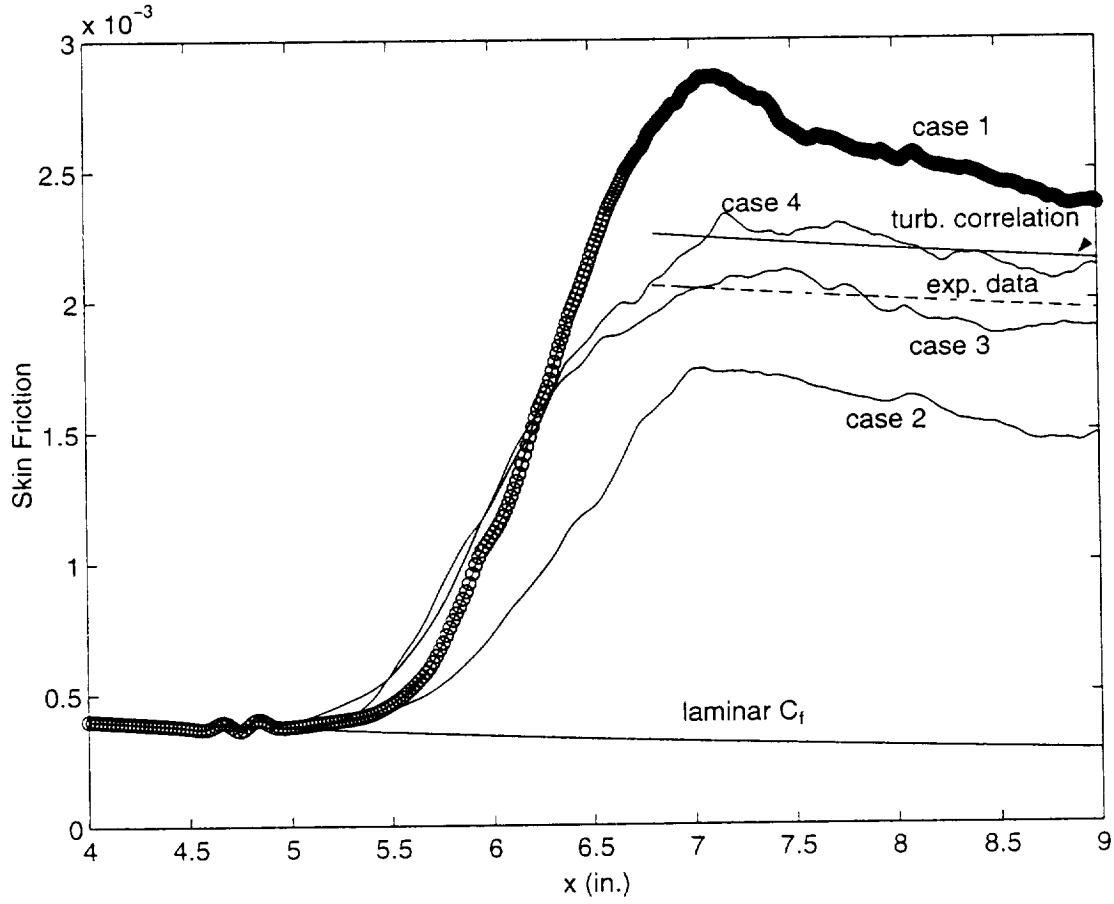

Figure 1: Streamwise evolution of the skin friction coefficient: effect of grid size.

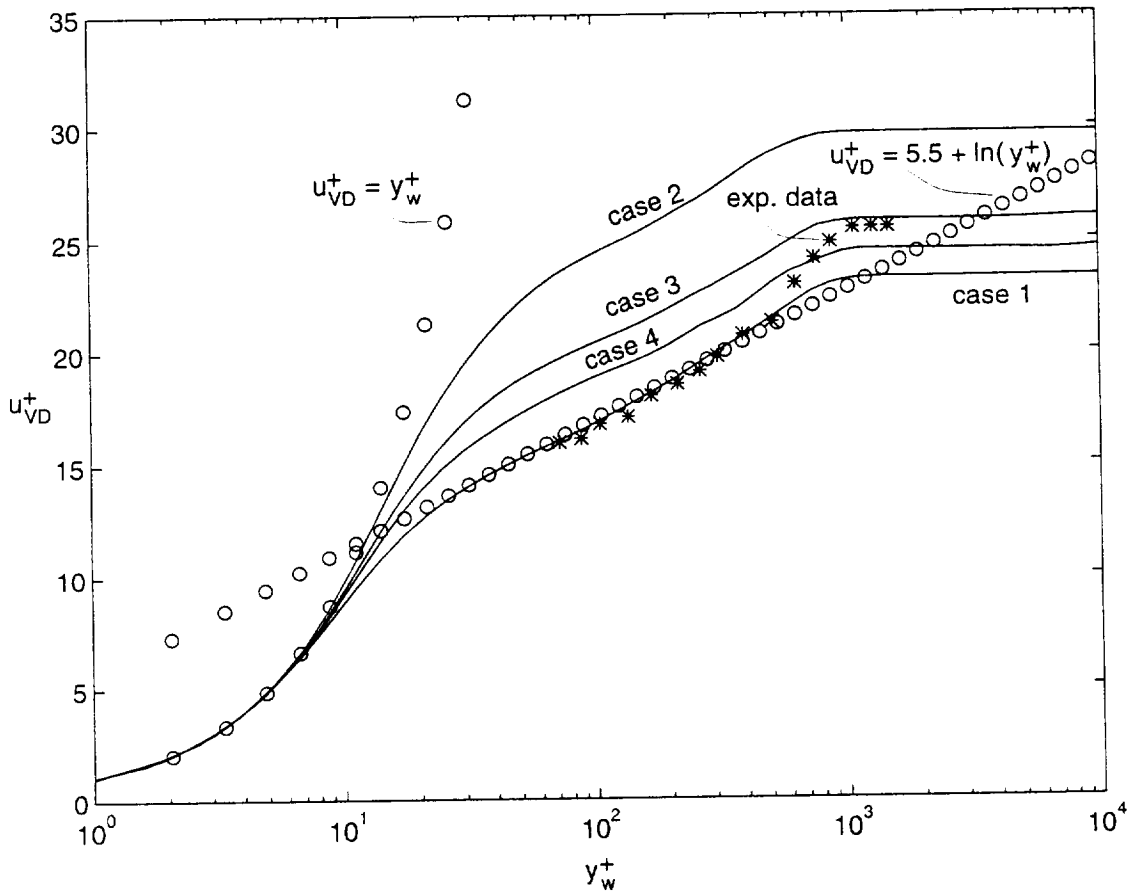

Figure 2: Profiles of Van Driest velocity normalized by wall-shear velocity at x=8.8in.; effect of grid size.

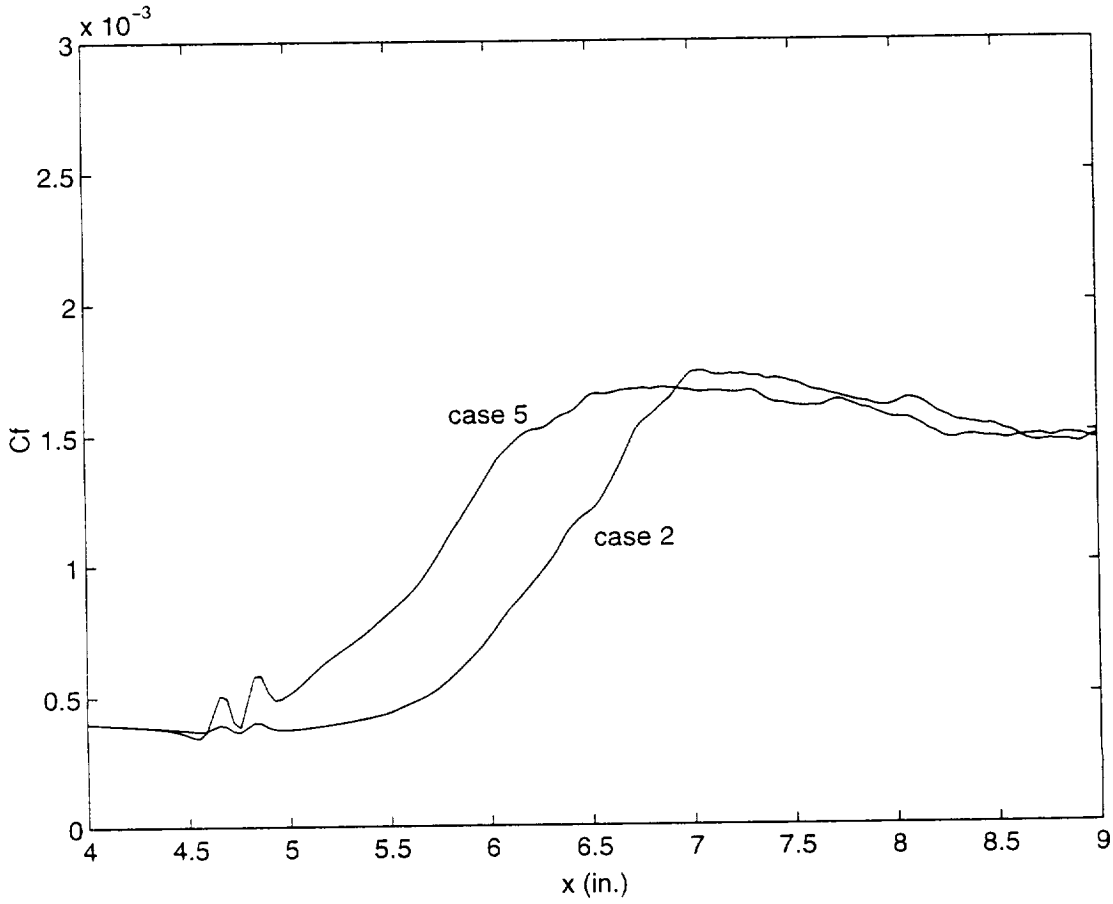

Figure 3: Streamwise evolution of the skin friction coefficient; effect of disturbance amplitude.

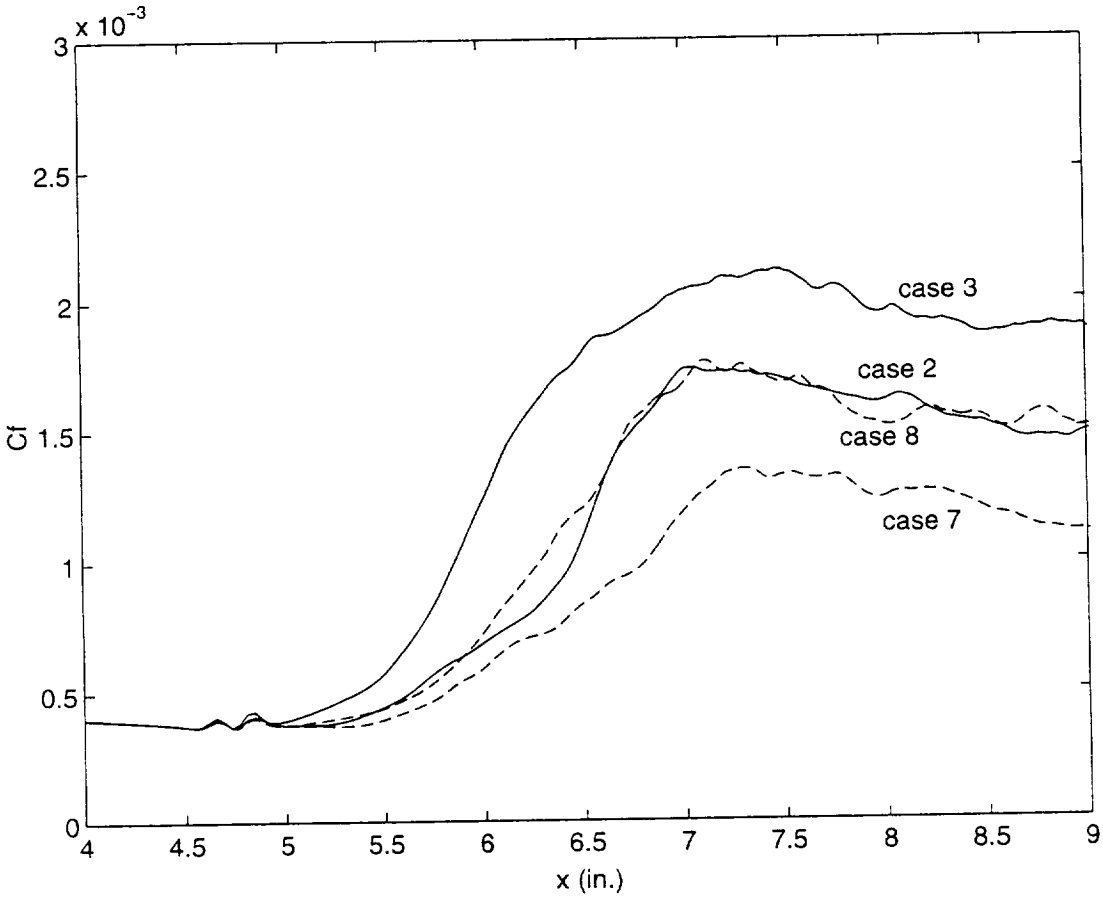

Figure 4: Streamwise evolution of the skin friction coefficient; effect of type of numerical scheme.